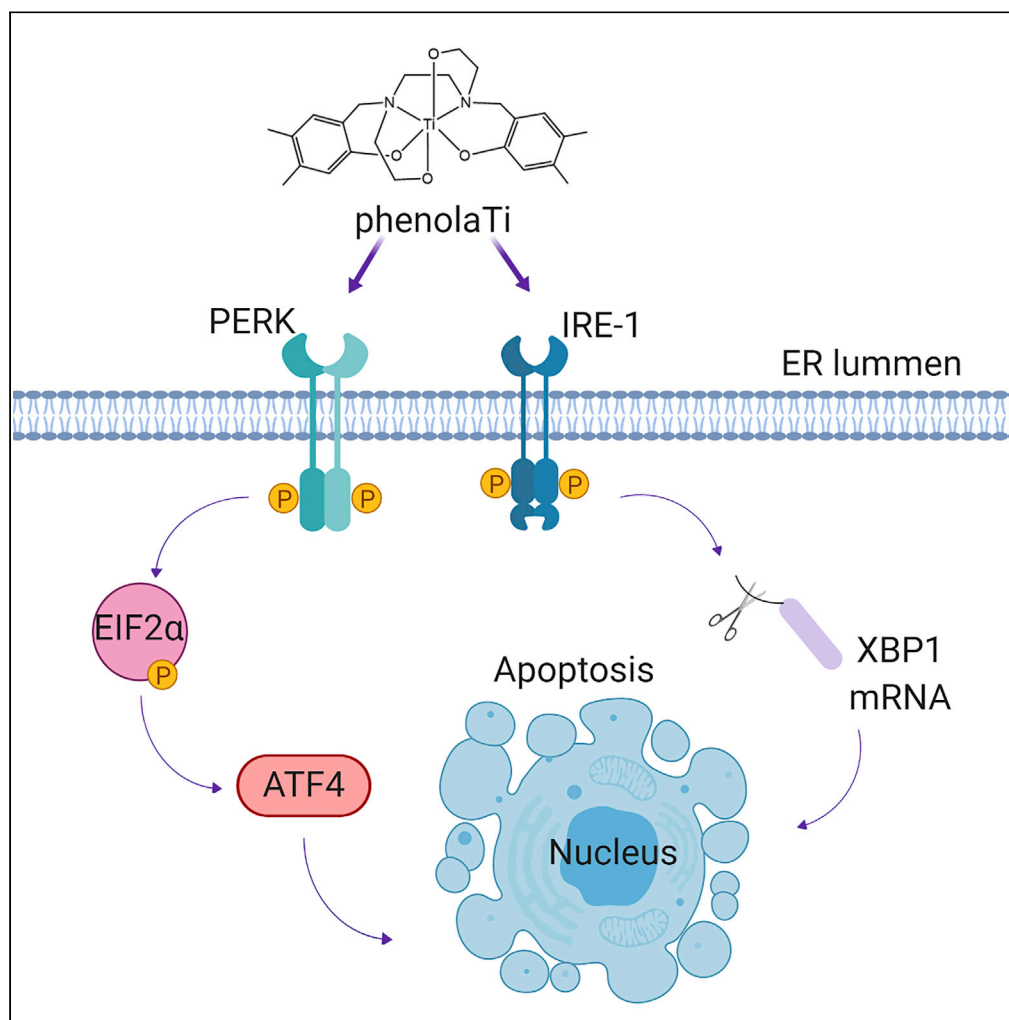


Article

Titanium Tackles the Endoplasmic Reticulum: A First Genomic Study on a Titanium Anticancer Metallodrug



Maya Miller, Anna Mellul, Maya Braun, ..., Jacob Hochman, Edit Y. Tshuva, Yuval Tabach

edit.tshuva@mail.huji.ac.il (E.Y.T.)
yuvaltab@ekmd.huji.ac.il (Y.T.)

HIGHLIGHTS

First in-depth mechanistic analysis of a non-toxic Ti-based anticancer metallodrug

A comprehensive RNA-seq analysis to map the transcriptomic network initiated by phenolaTi.

Unraveling a distinct mechanism through ER stress, not through direct DNA binding

Toward understanding and applicability of diverse better-tolerable chemotherapies

Miller et al., iScience 23, 101262
July 24, 2020 © 2020 The Authors.
<https://doi.org/10.1016/j.isci.2020.101262>

Article

Titanium Tackles the Endoplasmic Reticulum: A First Genomic Study on a Titanium Anticancer Metallodrug

Maya Miller,^{1,2} Anna Mellul,^{2,4} Maya Braun,^{2,4} Dana Sherill-Rofe,² Emiliano Cohen,² Zohar Shpilt,¹ Irene Unterman,² Ori Braitbard,³ Jacob Hochman,³ Edit Y. Tshuva,^{1,5,*} and Yuval Tabach^{2,*}

SUMMARY

PhenolaTi is an advanced non-toxic anticancer chemotherapy; this inert bis(phenolato)bis(alkoxo) Ti(IV) complex demonstrates the intriguing combination of high and wide efficacy with no detected toxicity in animals. Here we unravel the cellular pathways involved in its mechanism of action by a first genome study on Ti(IV)-treated cells, using an attuned RNA sequencing-based available technology. First, phenolaTi induced apoptosis and cell-cycle arrest at the G2/M phase in MCF7 cells. Second, the transcriptome of the treated cells was analyzed, identifying alterations in pathways relating to protein translation, DNA damage, and mitochondrial eruption. Unlike for common metallodrugs, electrophoresis assay showed no inhibition of DNA polymerase activity. Reduced *in vitro* cytotoxicity with added endoplasmic reticulum (ER) stress inhibitor supported the ER as a putative cellular target. Altogether, this paper reveals a distinct ER-related mechanism by the Ti(IV) anticancer coordination complex, paving the way for wider applicability of related techniques in mechanistic analyses of metallodrugs.

INTRODUCTION

Chemotherapeutic drugs are essential in the treatment of a variety of cancers with mechanisms ranging from DNA alkylation to antimetabolites. Specifically, metallodrugs can serve as effective anti-neoplastic agents, as first discovered with the pioneering Pt-based drug cisplatin (CDDP). Nearly 50% of patients with cancer worldwide receive platinum-based drugs to cope with testicular, ovarian, head and neck, and other cancer types (Brabec et al., 2017; Komeda and Casini, 2012; Mjos and Orvig, 2014; Riddell and Lippard, 2018). The mode of action of cisplatin was widely explored and is presumed to involve interaction of the Pt center with the N atoms of the purine bases of adjacent DNA nucleotides, eventually leading to apoptosis (Riddell and Lippard, 2018). A limiting drawback of cisplatin and its derivatives, similarly to other chemotherapies, is the severe side effects accompanying their administration, resulting from toxicity to, among other things, the kidneys, liver, and brain. Other metals studied as alternatives include essential (Fe, Cu, Ni, Zn, etc.) and non-essential (Pt, Ru, Ti, etc.) elements, with Ti being the first non-platinum metal reaching clinical trials as an appealing candidate for anticancer chemotherapy.

The first generation of anticancer Ti(IV) compounds with diketonato- and cyclopentadienyl-based ligands showed activity both *in vitro* and *in vivo*, with reduced toxicity and side effects (Köpf and Köpf-Maier, 1979). Nevertheless, their utility in the clinic was hampered by rapid decomposition in biological environments (Caruso and Rossi, 2004; Caruso et al., 2001; Christodoulou et al., 1998; Cini et al., 2017; Ellahioui et al., 2017; Keppler et al., 1991; Koepf-Maier and Koepf, 1987; Loza-Rosas et al., 2017; Manohari Abeyasinghe and Harding, 2007; Meléndez, 2002; Ott and Gust, 2007; Peri et al., 2009; Toney and Marks, 1985; Tshuva and Ashenhurst, 2009; Tshuva and Miller, 2018), as occurs often with coordination complexes of the labile and oxophilic Ti(IV) metal. Insoluble and undefined O-bridged aggregates of different sizes and nuclearities are formed instantaneously upon interaction with water, leading to uncontrolled solution chemistry, difficult to monitor and analyze. Therefore, despite some mechanistic clues gained throughout the years, the cellular mode of action of these compounds is yet unknown (Cini et al., 2017). Still, a major benefit in using Ti(IV)-based coordination compounds is the biofriendly nature of the metal: its lability, although responsible for the rapid hydrolysis in biological environments, turns into an advantage with the ultimate hydrolysis product being the safe titanium dioxide, often found in a variety of daily products

¹Institute of Chemistry, The Hebrew University of Jerusalem, Jerusalem 9190401, Israel

²Department of Developmental Biology and Cancer Research, Institute of Medical Research-Israel-Canada, The Hebrew University of Jerusalem, Jerusalem 9112102, Israel

³Department of Cell and Developmental Biology, Alexander Silberman Institute of Life Science, The Hebrew University of Jerusalem, Jerusalem 9190401, Israel

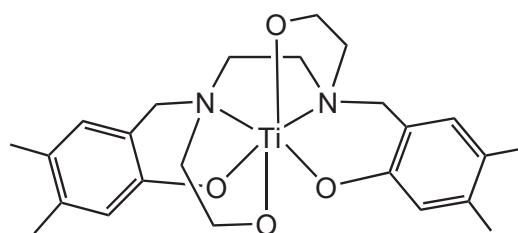
⁴These authors contributed equally

⁵Lead Contact

*Correspondence: edit.tshuva@mail.huji.ac.il (E.Y.T.), yuvaltab@ekmd.huji.ac.il (Y.T.)

<https://doi.org/10.1016/j.isci.2020.101262>





Scheme 1. PhenolaTi

(e.g., sunscreen, food coloring, drugs). Thus, advanced Ti(IV) coordination compounds with enhanced hydrolytic stability were developed to prolong the anticancer activity window before titanium dioxide is formed and is safely excreted. Specifically, the phenolato-based Ti(IV) complexes that we introduced showed a wide range of *in vitro* cytotoxic effects with no signs of *in vivo* toxicity; importantly, their high hydrolytic stability facilitates investigation of their molecular mechanisms of action (Barroso et al., 2015; Glasner and Tshuva, 2011, 2014; Immel et al., 2010, 2011, 2012; Manna et al., 2012; Meker et al., 2012, 2014, 2015; Miller et al., 2016; Peri et al., 2011a, 2011b; Shavit et al., 2007; Tinoco et al., 2012; Tshuva and Tzuberly, 2017; Tzuberly and Tshuva, 2012). In particular, we recently showed that a bis(phenolato)bis(alkoxo)Ti(IV) compound (phenolaTi, Scheme 1), conveniently synthesized from available starting materials, demonstrates high activity toward all cancer cell lines in the NCI-60 panel of the NIH with an average growth inhibition value (GI 50) of $4.6 \pm 2 \mu\text{M}$ (slightly better activity than cisplatin: $5.6 \mu\text{M}$; Figure S1) (Meker et al., 2016). No correlations in the cytotoxicity pattern to known drugs in the NIH database, as deduced from COMPARE analysis, implies a distinct mechanism of action. PhenolaTi also demonstrates the following: (1) high cytotoxicity toward cisplatin-resistant and multi-drug-resistant cell lines (Ganot and Tshuva, 2018; Meker et al., 2016); (2) *in vivo* efficacy with no indication of toxicity (Ganot et al., 2018); (3) high water stability for weeks in biological medium (Meker et al., 2016); (4) cellular accumulation and induction of apoptosis within 24–48 h following administration to human colon HT-29 cancer cells (Meker et al., 2016; Miller et al., 2016).

Herein we aimed to elucidate the mechanism of action of phenolaTi, as a lead anticancer complex, representative of Ti(IV)-based metallodrugs. To that effect, we applied RNA sequencing (RNA-seq) using CEL-Seq2 methodology (Hashimshony et al., 2016) on cell populations at different time points (up to 72 h) following exposure to the drug. Despite the significance of RNA-seq as a research tool, to our knowledge, only a single work used RNA-seq and a few more used microarray analyses to study the effect of metallodrugs (Bergamo et al., 2015; Grozav et al., 2015; Jovanović et al., 2016; Velma et al., 2016), whereby no studies were reported on Ti(IV) cytotoxicity pathways. Genes related to cell-cycle checkpoints, protein translation, and the endoplasmic reticulum (ER) pathway were significantly altered, thus introducing the first indication of ER involvement in the distinct action of anticancer Ti(IV) phenolato compounds.

RESULTS

To perform in-depth mechanistic analysis of phenolaTi, we aimed to map its dose- and time-dependent effects on the MCF7 human breast adenocarcinoma cell line and analyze the cellular behavior (Figure 1). Breast cancer is the most frequent malignancy in females; therefore, MCF7 cells are widely employed as an *in vitro* model in cancer research (Comşa et al., 2015) and were thus selected for this study. PhenolaTi was synthesized as previously described, from $\text{Ti}(\text{O}i\text{Pr})_4$ and the ligand precursor; the latter had been synthesized by a single-step condensation reaction from available starting materials (Meker et al., 2016). Preliminary cytotoxicity studies showed no evident toxicity for the first 6 h of exposure and maximal effect was detected at 72 h (Figure S2). Therefore, we incubated the cells with phenolaTi ($54 \mu\text{M}$; selected according to the cytotoxicity curves; Figure S2) and analyzed cell-cycle effects, cytotoxicity, apoptosis, and expression profiles, untreated (time 0) and after 3, 6, 15, 24, and 48 h of exposure.

PhenolaTi Induces Apoptosis and Cell-Cycle Arrest

The effect of phenolaTi on MCF7 cells was first measured using flow cytometry to determine cell kinetics, proliferation, and apoptosis. Cells accumulated at the G2/M phase (from 27% to 42%; whereby some accumulation also at S phase can't be ruled out) with major reduction in the percentage of cells in the G1 phase (from 67% to 49%) (Figures 2A and S3A), suggesting inhibition of cell-cycle checkpoints. Additionally,

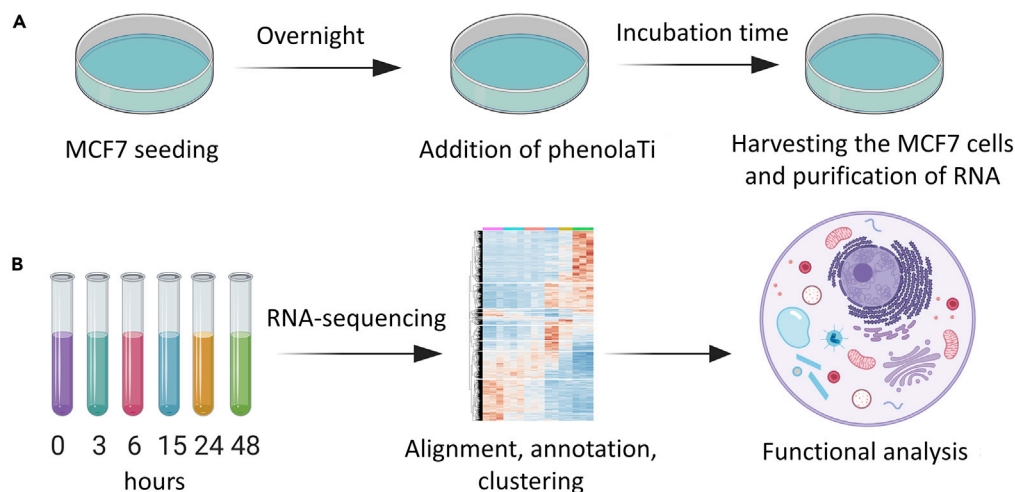


Figure 1. General Experimental Procedure

(A) Experimental *in vitro* workflow; MCF7 cells were seeded overnight, phenolaTi was added at 54 μM at different time points, harvesting was generated at the same time point to obtain 3, 6, 15, 24, and 48 h of incubation (with untreated control samples, 0). (B) Generated samples were sequenced, aligned, annotated, clustered, and functionally analyzed. MCF7 cells undergo changes in response to phenolaTi treatment.

apoptosis induction was evident: (1) double staining with Annexin V-FITC and propidium iodide (PI) revealed an increase in the percentage of late and early apoptotic cells within 24 h (Figures 2B and S3B); (2) characteristic morphological changes indicative of regulated cell death were detected (Figure 2C). These observations overall point to regulated, programmed cellular death executed by the cellular machinery in response to treatment with phenolaTi (Manna et al., 2012; Meeker et al., 2016; Miller and Tshuva, 2018; Miller et al., 2016).

Cellular Pathways Identified by Transcriptomic Characterization

After establishing the effect of phenolaTi on cell viability and proliferation, we aimed to offer a plausible mechanism of action by mapping transcriptomic changes following phenolaTi treatment, namely, changes in transcribed mRNA molecules. To that effect, MCF7 cells were treated with phenolaTi (54 μM) and incubated for 0 (untreated), 3, 6, 15, 24, and 48 h in triplicates. Then, the mRNA was extracted and sequenced. Both upregulation and downregulation compared with time zero (untreated cells) were considered for analysis, as shown in the heatmap. The 5,000 most variably expressed genes were further analyzed. These genes were divided into five main clusters, applying hierarchical clustering methodology to group similarly behaving genes (Figure 3).

The five clusters, according to their pattern of expression, are the following (Figure 3) (large to small): (1) cluster (I) of 1,426 genes that were upregulated at 48 h; (2) cluster (V) of 1,284 genes that were downregulated within 3 h; (3) cluster (II) of 684 genes that were upregulated at 15 h; (4) cluster (III) of 406 genes that were locally upregulated at 15 h; (5) cluster (IV) of 251 genes that were downregulated at 15 h. GeneAnalytics (Ben-Ari Fuchs et al., 2016) was employed to annotate the genes in each cluster and associate it with the biological function. Figure 3 presents the most relevant results; full data are provided in the Supplemental Information (Table S1).

The first event following exposure to phenolaTi was downregulation within 3 h and then low expression across all time points (Figure 3 cluster (V)). The genes in this cluster are significantly associated with DNA repair (p value $< 3.79 \times 10^{-8}$) and cell cycle (p value $< 2.07 \times 10^{-10}$) (e.g., CHEK2, RAD51, BRIP1, and FANCL). The second transcriptional event was downregulation of mitochondrial translation genes after a 15-h incubation period (Figure 3 cluster (IV)). Simultaneously, temporary upregulation was observed of genes related to different mitochondrial processes (e.g., respiration, electron transport, ATP synthesis), as well as those related to ribosome subunits and other proteins required for translation (Figure 3 cluster (III)). From the 15th h onward upregulation of multiple translational processes included genes associated with ER and the ribosome, which were constantly high (Figure 3 cluster (II)). These processes include

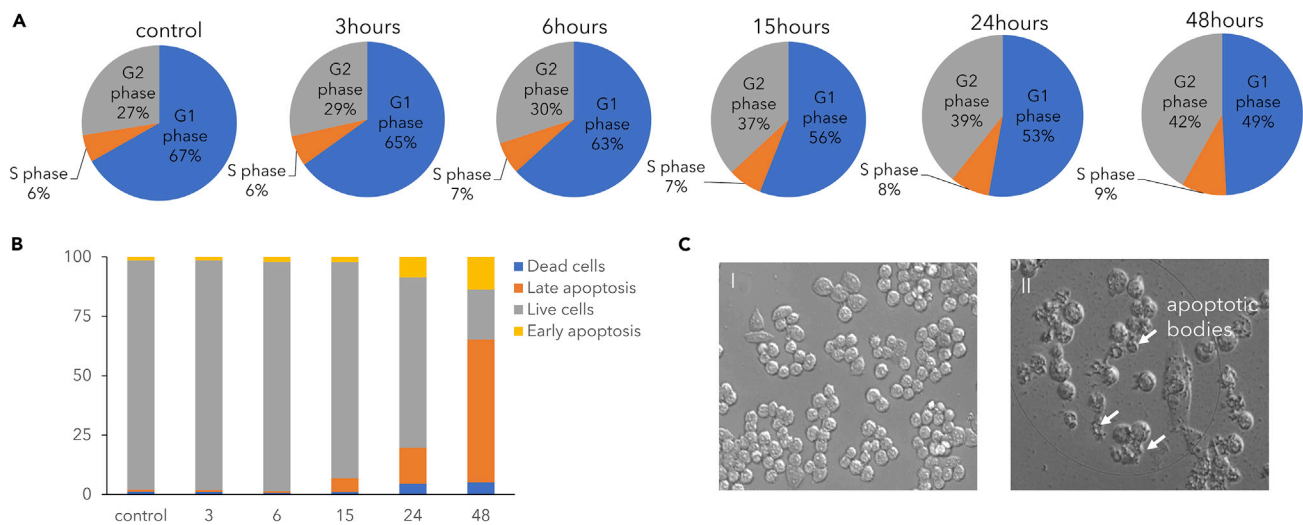


Figure 2. MCF7 Cells undergo Changes in Response to PhenolaTi Treatment

(A) Cell-cycle distribution following incubation with phenolaTi at 54 μM at different time points. (B) Time-dependent effect of phenolaTi at 54 μM on apoptosis in MCF7 cancer cells, as recorded using flow cytometry. (C) Microscopic images of MCF7 cells (I) untreated cells, control (II) treated with phenolaTi at 54 μM for 36 h of incubation. Gene expression alteration in response to phenolaTi in MCF7 cells.

cytoplasmic translation, ribosomal small/large subunit assembly and biogenesis and translational elongation. Lastly, at 48 h time, mRNA transcription, transport, and splicing were also upregulated (Figure 3 cluster (I)). Among the most significantly altered genes during the course of the measurement were ATXN7 (p value 6.4×10^{-14}), GABRA2 (p value 2.4×10^{-11}), and PLCG2 (p value 7.3×10^{-12}), which relate to ER processes (Dai et al., 2009; Kurosaki et al., 2000; Nagy et al., 2009).

The transcriptomic analysis correlated with the cell cycle and apoptosis experiments (Figures 2 and 3). As supported by flow cytometry, genes related to cell cycle were affected (Figure 3 cluster (III)/(IV)), such as cyclin dependent kinase 1 (CDK1), responsible for progression of cells into the M phase (DiPaola, 2002; Kha-zaei et al., 2017; Wang et al., 2016), which is downregulated within 3 h (Figure 3 cluster (V)). Moreover, proapoptotic genes, such as Growth Arrest and DNA Damage 45 (GADD45) and Activating Transcription Factor 4 (ATF4) were upregulated within 48 h (Figure 3 cluster (I)), in agreement with the observed changes (Figures 2B and 2C). Importantly, ATF4 is a key player in the cellular response to hypoxia evolved in ER stress (Rzymiski et al., 2009).

Overall, phenolaTi treatment upregulated processes related to the translation of proteins in the ER and ribosomal biogenesis (Figure 3 cluster (II)/(III)). A variety of ribosomal genes (RPL and RPS) were upregulated within 15 h, among which some were consequently downregulated, and others were continuously highly expressed at 24/48 h. Moreover, significant upregulation of EIF3C gene (p value 6.7×10^{-7}) was observed, a key player in translation initiation within cells (Wagner et al., 2014); together with high expression of ATF4, this observation supports involvement of ribosome and ER in the cellular response to phenolaTi.

Short-Term Effect (3–15 h) of PhenolaTi Supports Hypoxia and ER Stress

The analysis points to major changes in gene expression, mainly observed 15 h or more following treatment. To focus on the short-term effect of the drug, gene expression in the first 15 h following exposure (3, 6, and 15 h) was specifically analyzed relative to control (0 h), looking at genes most variable at short time points (Figure S4). The most significantly altered gene already within 3 h of exposure was SLC30A1 (p value 4.7×10^{-35}), associated with cation transmembrane activity; interestingly, this gene is involved in zinc efflux through the ER membrane (Barresi et al., 2018). Additional altered genes within 6 h of exposure include EGLN2 (p value 4.66×10^{-6}), involved in oxygen sensing related to hypoxia tolerance; PNRC2 (p value 5.6×10^{-24}), associated with energy balance/storage; and TMEM177 (p value 2.2×10^{-22}), a mitochondrial respiratory chain complex assembly factor. This gene signature further supports the effect on mitochondria previously observed for related Ti phenolato compounds, accumulated in the mitochondria organelle (Schur et al., 2013). Inspecting the genes altered within 15 h of treatment, the

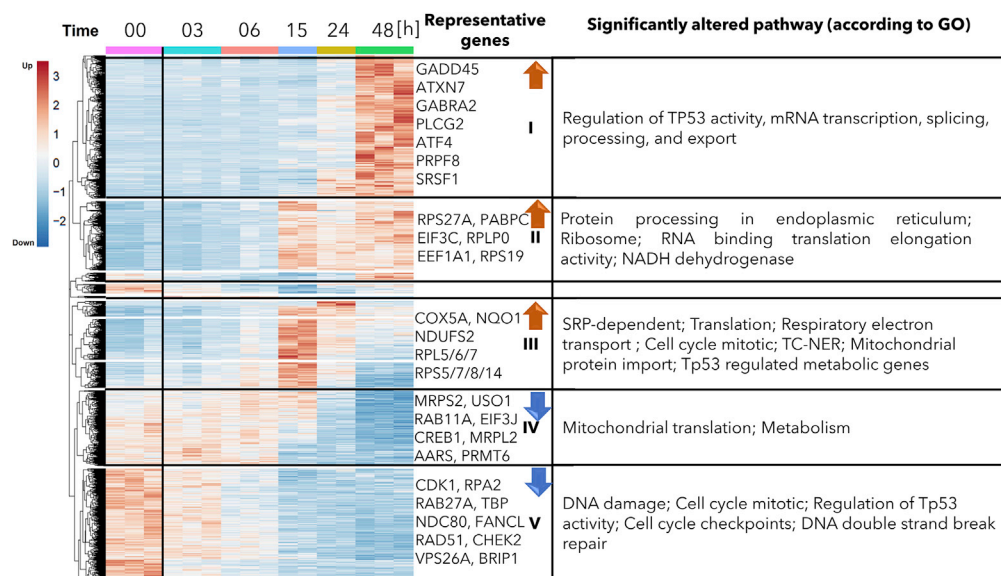


Figure 3. Gene Expression (RPM, Reads per Million) Alteration in Response to PhenolaTi in MCF7 Cells at 54 μ M
MCF7 were treated with 54 μ M phenolaTi and sequenced in triplicates or duplicates after 0 (untreated), 3, 6, 15, 24, and 48 h. Expression analysis included CEL-seq2, Z-scoring, and hierarchical clustering. Roughly, the genes can be divided into five main clusters with distinct expression and significant biological functions. The biological functions of the genes were analyzed using GeneAnalytics, an integrative gene set analysis tool (Ben-Ari Fuchs et al., 2016). Blue, increased gene expression; red, decreased gene expression. Changes in expression of ER/hypoxia-related genes in response to phenolaTi in MCF7 cells.

downregulated genes relate to cell-cycle checkpoints (e.g., CDC23) and DNA damage (e.g., BRCA1). Overall, examining the most significant genes over the entire short time course of 3/6/15 h, three genes are constantly upregulated: CYP1A1, SLC30A1, and PYGM (Figures S4D and S4E). The first two genes relate to cellular response to metal ions (Chen and Chan, 2016; Zogzas and Mukhopadhyay, 2018), whereby CYP1A1 is a member of cytochrome p450 superfamily enzymes, which are localized mainly in the inner membrane of the mitochondria or the ER and are associated with cancer susceptibility (Agúndez, 2004; Brignac-Huber et al., 2016; Kawajiri et al., 1993; Sharma et al., 2014). The alterations in CYP1A1 together with those of SLC30A1 again focused our attention specifically on the ER as a putative cellular target.

Analysis of Pathway-Related Genes: PhenolaTi Causes Changes in Hypoxia and Endoplasmic Reticulum-Related Genes

Known metallodrugs, particularly cisplatin and its Pt-based derivatives, operate by direct DNA binding (Meier-Menches et al., 2018; Riddell and Lippard, 2018). For any similarly operating metallodrug, upregulation of genes related to DNA damage would be expected, such as the homologous recombination repair (HRR)-related genes. In contrast, our data show downregulation of DNA damage-related genes (Figure 3 cluster (V)). This indication implies that direct DNA damage is not induced by phenolaTi. Nonetheless, previous studies showed connection between downregulation of HRR genes and hypoxia (Bindra et al., 2004, 2005; Chan et al., 2008; Meng et al., 2005), which in turn can correlate with ER stress.

Owing to the aforementioned results, we evaluated specifically the possible induction of hypoxic mimetic conditions by phenolaTi. Interestingly, from a set of 51 genes previously reported to be strongly related to hypoxia (Buffa et al., 2010), 26 genes were significantly altered herein (p value < 0.0005 based on hypergeometric distribution) (Figure 4A). Of these 26 genes, 12 were strongly upregulated within 15 h and the rest were downregulated. The downregulated genes are annotated to mitochondrial translation processes, whereas the upregulated genes relate to the glucose metabolism pathway or hypoxia inducing factor 1 (HIF1) signaling pathway (Figure 4B), further supporting phenolaTi-induced hypoxia. The mechanism by which phenolaTi mimics hypoxia induction remains to be elucidated; but it may also relate to the altered expression of mitochondrial genes and reduction in oxygen levels (Figure 3 clusters (III)/(IV)).

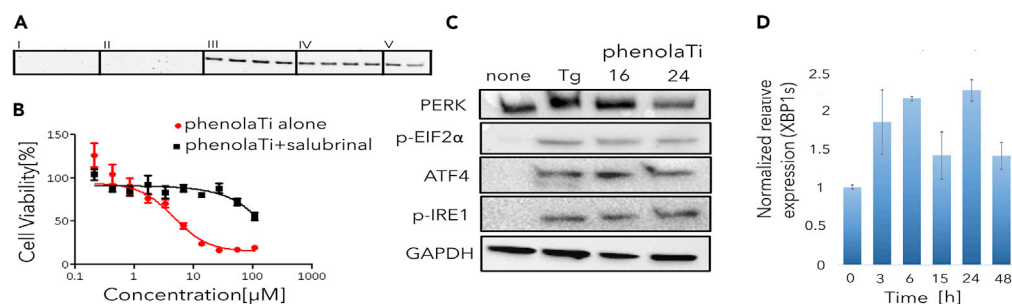


Figure 5. In Vitro Validation Assays Support ER-Related Mechanism of PhenolaTi with No Direct DNA Binding

(A) Agarose gel electrophoresis of the PCR products for detection of actin after co-incubation with (I) cisplatin, (II) doxorubicin, (III) 5-fluorouracil, (IV) phenolaTi, (V) control, at 27 (left 2 bands) or 54 (right 2 bands) μM of each tested compound in duplicates (showing one of three repeats); phenolaTi, as 5-fluorouracil, does not interact directly with DNA. (B–D) (B) Cytotoxicity curves of phenolaTi toward human MCF7 cancer cells, with and without the addition of salubrinal, using the MTT assay following 72 h of incubation; activity of phenolaTi is abolished with the ER-stress inhibitor. (C) Expression of PERK, p-EIF2 α , ATF4, and p-IRE1 levels (evaluated using immunoblotting) in MCF7 cells following incubation with phenolaTi; positive control Thapsigargin (Tg, a known ER Ca²⁺ ATPase inhibitor; 4 nM for 16 h); GAPDH as a loading control (inactivated PERK is observed at a lower molecular weight at time point 0, whereas activated PERK is observed upon treatment). (D) qPCR levels of XBP1s form over time in MCF7 cells exposed to phenolaTi at 54 μM concentration.

Yang and Wang, 1999). In contrast, 5-fluorouracil is a thymidylate synthase inhibitor (Rustum et al., 1997) and hence served as a negative control. DNA was isolated from MCF7 cancer cells at a concentration of 0.4 ng/ μL , amplifying the fragments of the gene that codes for actin. The tested compounds at concentrations of 27 and 54 μM were separately added to PCR tubes for evaluation of possible interaction with DNA, by inspecting inhibition of the DNA polymerase activity, as manifested by inhibition of gene amplification. The results are depicted in Figure 5A. As expected, the actin bands were absent for the drugs operating on DNA: cisplatin and doxorubicin, indicative of inhibition to the DNA polymerase activity due to DNA-drug interaction. The well-detected bands for 5-fluorouracil and phenolaTi imply that, as for fluorouracil, DNA may not be the major target of Ti(IV) phenolato compounds in their cytotoxic effect, supporting the transcriptomics data.

The gene expression analysis pointed to ER as a target involved in the mechanism of action of phenolaTi. ER stress is characterized by disruption of ER homeostasis, which is responsible mainly for production and folding of cellular proteins, storage and regulation of calcium, and glucose metabolism. In response to ER stress, the cell activates a signaling pathway called the unfolded protein response (UPR), which aims to help the cell cope with the induced stress. There are three major sensors (proteins) controlling the UPR: inositol requiring enzyme 1 (IRE1), protein kinase RNA-activated (PKR)-like ER kinase (PERK), and activating transcription factor 6 (ATF6). IRE1 activation induces X-box binding protein 1 (XBP1) splicing. The downstream proteins of PERK are eukaryotic initiation factor 2 (EIF2) and activating transcription factor 4 (ATF4) proteins.

To further analyze the effect of phenolaTi on ER stress as suggested by the transcriptomics, the cytotoxicity of phenolaTi was tested on MCF7 breast adenocarcinoma cells, with and without 70 μM of salubrinal, a known ER-stress inhibitor (Boyce et al., 2005; Suntharalingam et al., 2013, 2014) that inhibits eIF2 α dephosphorylation, using the MTT assay (Ganot et al., 2013). The results are presented in Figure 5B.

The activity of phenolaTi was abolished in the presence of salubrinal. The protective effect of salubrinal on cell viability suggests that ER stress has a role in inducing cell death. We then aimed to characterize the alterations in the different components of the phenolaTi-induced ER-stress response pathway. As mentioned above, there are three main ER-stress regulating proteins: IRE1, PERK, and ATF6. Their activation has both pro-apoptotic and pro-survival effects, depending on stress duration and intensity. At ~16 and 24 h post phenolaTi treatment, activated IRE1 and XBP1s expression was observed (Figures 5C and 5D). Additionally, activated PERK leads to phosphorylation of the protein Eif2 α and, in turn, to ATF4 translation. Again, activated PERK and Eif2 α phosphorylation were detected along with ATF4 expression at the same time points (Figure 5C). These results strongly support the hypothesis pointing

to ER as at least one of the main molecular targets associated with the apoptotic cell death induced by phenolaTi.

DISCUSSION

In this study, we present the first in-depth mechanistic analysis of a Ti(IV)-based anticancer drug. The scarce genomic analyses reported previously for Pt- and Ru-based metallodrugs involved microarray or conventional RNA-seq methodologies (Bergamo et al., 2015; Grozav et al., 2015; Jovanović et al., 2016; Velma et al., 2016). Herein, the advanced CEL-Seq2 methodology (Hashimshony et al., 2016), which has optimized primers, reagents, clean-up, and library preparation steps, was employed on cell populations rather than applied as a single-cell sequencing technique, enabling conveniently gaining new insights on the pathways involved within the mode of action of the Ti(IV) drug.

A variety of essential signaling pathways were significantly changed over the tested time course. Cell cycle was erupted at G2/M phase, and apoptosis initiation via a mitochondrial pathway is proposed based on microscopically detected changes, buildup of apoptotic cells, and alterations in mitochondria-related genes, all in agreement with some reports in the literature on mechanistic aspects of Ti-based metallodrugs (Manna et al., 2012; Meker et al., 2016; Miller et al., 2016). All of the above support a well-programmed cell death initiated by phenolaTi.

Inspecting correlations to the genomic analyses of other anticancer metallodrugs (Bergamo et al., 2015; Grozav et al., 2015; Jovanović et al., 2016; Velma et al., 2016), it is evident that, despite some similarities relating to apoptosis induction, cell-cycle arrest, and p53-based mediated pathways, phenolaTi operates distinctively as implied previously by the NCI-60 reactivity pattern (Meker et al., 2016). The ancestor drug cisplatin operates directly on DNA (Riddell and Lippard, 2018; Wang and Lippard, 2005), whereas the downregulation of DNA double-strand break pathway within the first hours of exposure to phenolaTi suggests fundamentally different cellular behaviors. The lack of interference with DNA polymerase activity also supports an indirect interaction between phenolaTi and DNA under the tested conditions. Interestingly, downregulation of DNA repair genes is associated with hypoxic conditions in cells (Bindra et al., 2004, 2005; Chan et al., 2008; Meng et al., 2005), which was corroborated through direct analysis of hypoxia-related genes (Buffa et al., 2010). Also, when comparing the results with those previously reported for Ru-based compounds, phenolaTi does not activate similar metastasis-related TFs (Bergamo et al., 2015), thus further confirming its distinct cellular impact.

The main pathways that stand out as particularly influenced by phenolaTi are those related to the ER, as proposed previously for osmium-based anticancer drugs (Boyce et al., 2005; Suntharalingam et al., 2013, 2014). A variety of proteins and metabolic processes were altered, ATF4 was identified in one cluster (up-regulation at 48 h), and genes associated with ER function based on previous work were upregulated following phenolaTi treatment. Notably, *in vitro* cytotoxicity toward MCF7 cells was abolished upon addition of salubrinal, a known ER-stress inhibitor (Boyce et al., 2005), which further supports ER involvement in the mechanism of action of phenolaTi. Upregulation of both IRE1 and PERK pathways further validate ER-stress activation. Interestingly, previous cell imaging studies with fluorescent salen-type Ti(IV) complexes have suggested possible accumulation of the fluorescent species near the ER region in the cell (Tzuberly et al., 2018). Since the ER membrane mainly comprises phospholipids (Brignac-Huber et al., 2016), direct interaction of the oxophilic Ti(IV) metal with the ER to give strong Ti(IV)-phosphate bonds is plausible, although such interaction would not be ER specific.

To conclude, unlike cisplatin and related known drugs, ER stress and hypoxia appear to govern Ti(IV)-based cytotoxic reactivity, conditions that could be related (Corazzari et al., 2017; Pereira et al., 2014). Nevertheless, additional pathways activated in parallel or on different lines/by different derivatives cannot be ruled out. The specific interactions between the drug and its direct target are yet to be elucidated, as well as the source for cancer selectivity as manifested by the unique combination of wide activity and no toxic effects for phenolaTi (Ganot et al., 2018). ATF4 was previously reported to contribute to tumor progression (Fels and Koumenis, 2006), as well as malfunction or overexpression of phosphorylation process (Ardito et al., 2017), all of which may serve a plausible explanation for cancer selectivity observed *in vivo* for phenolaTi. Overall, being a highly promising new-generation anticancer chemotherapeutic drug, the mechanistic insights provided herein for phenolaTi promote the understanding and advancing of modern non-toxic chemotherapy. Lastly, the wide applicability and availability of the RNA-seq methodology applied on

cell populations as described herein should progress more rapid, economical, and in-depth mechanistic analyses of various metallodrugs operating by various mechanisms, for a marked leap in cancer research and better accessibility of various tolerable chemotherapies.

Limitations of the Study

The study was performed on breast adenocarcinoma MCF7 cell line and therefore is limited by the mutational status of the current tested cells.

Resource Availability

Lead Contact

Further information and requests for resources and reagents should be directed to and will be fulfilled by the Lead Contacts, Edit Y. Tshuva (edit.tshuva@mail.huji.ac.il) and Yuval Tabach (yuvaltab@ekmd.huji.ac.il).

Materials Availability

This study did not generate new unique reagents.

Data and Code Availability

The raw and the processed data files of the current study can be accessed through Gene Expression Omnibus (GEO) with the GSE148239 accession number.

METHODS

All methods can be found in the accompanying [Transparent Methods supplemental file](#).

SUPPLEMENTAL INFORMATION

Supplemental Information can be found online at <https://doi.org/10.1016/j.isci.2020.101262>.

ACKNOWLEDGMENTS

We thank Mohamed Mahameed for his fruitful discussion regarding the endoplasmic reticulum response. Funding was received from the European Research Council (ERC) under the European Union's Horizon 2020 Research and Innovation Program (grant agreement 681243), The U.S.- Israel Binational Science Foundation (BSF) (grant agreement 0375055), and the Israel Science Foundation (ISF) (grant agreement 1591/19), Melanoma Research Association (grant agreement 402792).

AUTHOR CONTRIBUTIONS

Conceptualization, M.M., E.Y.T., and Y.T.; Investigation, M.M., A.M., M.B., E.C., Z.S., E.Y.T., and Y.T.; Data curation and software, E.C. and M.M.; Writing - Original Draft, M.M. and E.Y.T.; Writing - Review and Editing, M.M., D.S.-R., I.U., O.B., J.H., E.Y.T., and Y.T.; Funding acquisition, E.Y.T.; Resources, Y.T. and E.Y.T.

DECLARATION OF INTERESTS

The authors declare no competing interests. Relating patent: Tshuva EY and Hochman J; Cytotoxic titanium and vanadium complexes PCT/IL2013/05,069 filled 15/08/2013.

Received: February 16, 2020

Revised: May 7, 2020

Accepted: June 5, 2020

Published: July 24, 2020

REFERENCES

- Agúndez, J.A.G. (2004). Cytochrome P450 gene polymorphism and cancer. *Curr. Drug Metab.* 5, 211–224.
- Ardito, F., Giuliani, M., Perrone, D., Troiano, G., and Lo Muzio, L. (2017). The crucial role of protein phosphorylation in cell signaling and its use as targeted therapy. *Int. J. Mol. Med.* 40, 271–280.
- Barresi, V., Valenti, G., Spampinato, G., Musso, N., Castorina, S., Rizzarelli, E., and Condorelli, D.F. (2018). Transcriptome analysis reveals an altered expression profile of zinc transporters in colorectal cancer. *J. Cell Biochem.* 119, 9707–9719.
- Barroso, S., Coelho, A.M., Gomez-Ruiz, S., Calhorda, M.J., Zizak, Z., Kaluderovic, G.N., and Martins, A.M. (2015). Correction: synthesis, cytotoxic and hydrolytic studies of titanium

complexes anchored by a tripodal diamine bis(phenolate) ligand. *Dalt. Trans.* **44**, 2497.

Ben-Ari Fuchs, S., Lieder, I., Stelzer, G., Mazor, Y., Buzhor, E., Kaplan, S., Bogoch, Y., Plaschkes, I., Shitrit, A., and Rappaport, N. (2016). GeneAnalytics: an integrative gene set analysis tool for next generation sequencing, RNA-seq and microarray data. *Omi. A J. Integr. Biol.* **20**, 139–151.

Bergamo, A., Gerdol, M., Lucafo, M., Pelillo, C., Battaglia, M., Pallavicini, A., and Sava, G. (2015). RNA-seq analysis of the whole transcriptome of MDA-MB-231 mammary carcinoma cells exposed to the antimetastatic drug NAMI-A. *Metallomics* **7**, 1439–1450.

Bindra, R.S., Schaffer, P.J., Meng, A., Woo, J., Mäseide, K., Roth, M.E., Lizardi, P., Hedley, D.W., Bristow, R.G., and Glazer, P.M. (2004). Down-regulation of Rad51 and decreased homologous recombination in hypoxic cancer cells. *Mol. Cell. Biol.* **24**, 8504–8518.

Bindra, R.S., Gibson, S.L., Meng, A., Westermarck, U., Jasin, M., Pierce, A.J., Bristow, R.G., Classon, M.K., and Glazer, P.M. (2005). Hypoxia-induced down-regulation of BRCA1 expression by E2Fs. *Cancer Res.* **65**, 11597–11604.

Boyce, M., Bryant, K.F., Jousse, C., Long, K., Harding, H.P., Scheuner, D., Kaufman, R.J., Ma, D., Coen, D.M., and Ron, D. (2005). A selective inhibitor of eIF2 α dephosphorylation protects cells from ER stress. *Science* **307**, 935–939.

Brabec, V., Hrabina, O., and Kasparkova, J. (2017). Cytotoxic platinum coordination compounds. DNA binding agents. *Coord. Chem. Rev.* **351**, 2–31.

Brignac-Huber, L.M., Park, J.W., Reed, J.R., and Backes, W.L. (2016). Cytochrome P450 organization and function are modulated by endoplasmic reticulum phospholipid heterogeneity. *Drug Metab. Dispos.* **44**, 1859–1866.

Buffa, F.M., Harris, A.L., West, C.M., and Miller, C.J. (2010). Large meta-analysis of multiple cancers reveals a common, compact and highly prognostic hypoxia metagene. *Br. J. Cancer* **102**, 428.

Caruso, F., and Rossi, M. (2004). Antitumor titanium compounds and related metalocenes. *Met. Ions Biol. Syst.* **42**, 353–384.

Caruso, F., Rossi, M., and Pettinari, C. (2001). Anticancer titanium agents. *Expert Opin. Ther. Patents* **11**, 969–979.

Chan, N., Koritzinsky, M., Zhao, H., Bindra, R., Glazer, P.M., Powell, S., Belmaaza, A., Wouters, B., and Bristow, R.G. (2008). Chronic hypoxia decreases synthesis of homologous recombination proteins to offset chemoresistance and radioresistance. *Cancer Res.* **68**, 605–614.

Chen, Y.Y., and Chan, K.M. (2016). Differential effects of metal ions on TCDD-induced cytotoxicity and cytochrome P4501A1 gene expression in a

zebrafish liver (ZFL) cell-line. *Metallomics* **8**, 236–251.

Christodoulou, C., Eliopoulos, A., Young, L., Hodgkins, L., Ferry, D., and Kerr, D. (1998). Antiproliferative activity and mechanism of action of titanocene dichloride. *Br. Journal Cancer* **77**, 2088–2097.

Cini, M., Bradshaw, T.D., and Woodward, S. (2017). Using titanium complexes to defeat cancer: the view from the shoulders of titans. *Chem. Soc. Rev.* **46**, 1040–1051.

Comşa, Ş., Cimpean, A.M., and Raica, M. (2015). The story of MCF-7 breast cancer cell line: 40 years of experience in research. *Anticancer Res.* **35**, 3147–3154.

Corazzari, M., Gagliardi, M., Fimia, G.M., and Piacentini, M. (2017). Endoplasmic reticulum stress, unfolded protein response, and cancer cell fate. *Front. Oncol.* **7**, 78.

Dai, J., Wang, X., Chen, Y., Wang, X., Zhu, J., and Lu, L. (2009). Expression quantitative trait loci and genetic regulatory network analysis reveals that Gabra2 is involved in stress responses in the mouse. *Stress* **12**, 499–506.

DiPaola, R.S. (2002). To arrest or not to G2-M Cell-cycle arrest. *Clin. Cancer Res.* **8**, 3512–3519.

Ellahioui, Y., Prashar, S., and Gomez-Ruiz, S. (2017). Anticancer applications and recent investigations of metallodrugs based on gallium, tin and titanium. *Inorganics* **5**, 4.

Fels, D.R., and Koumenis, C. (2006). The PERK/eIF2 α /ATF4 module of the UPR in hypoxia resistance and tumor growth. *Cancer Biol. Ther.* **5**, 723–728.

Ganot, N., and Tshuva, E.Y. (2018). In vitro combinations of inert phenolato Ti (iv) complexes with clinically employed anticancer chemotherapy: synergy with oxaliplatin on colon cells. *RSC Adv.* **8**, 5822–5827.

Ganot, N., Meker, S., Reytman, L., Tzuber, A., and Tshuva, E.Y. (2013). Anticancer metal complexes: synthesis and cytotoxicity evaluation by the MTT assay. *J. Vis. Exp.* **10**, e50767.

Ganot, N., Briaitbard, O., Gammal, A., Tam, J., Hochman, J., and Tshuva, E.Y. (2018). In vivo anticancer activity of a nontoxic inert phenolato titanium complex: high efficacy on solid tumors alone and combined with platinum drugs. *ChemMedChem* **13**, 2290–2296.

Glasner, H., and Tshuva, E.Y. (2011). A marked synergistic effect in antitumor activity of salan titanium(IV) complexes bearing two differently substituted aromatic rings. *J. Am. Chem. Soc.* **133**, 16812–16814.

Glasner, H., and Tshuva, E.Y. (2014). C-1-Symmetrical titanium(IV) complexes of salan ligands with differently substituted aromatic rings: enhanced cytotoxic activity. *Inorg. Chem.* **53**, 3170–3176.

Grozav, A., Balacescu, O., Balacescu, L., Cheminel, T., Berindan-Neagoe, I., and Therrien, B. (2015). Synthesis, anticancer activity, and genome profiling of thiazolo arene

ruthenium complexes. *J. Med. Chem.* **58**, 8475–8490.

Han, J., Back, S.H., Hur, J., Lin, Y.-H., Gildersleeve, R., Shan, J., Yuan, C.L., Krokowski, D., Wang, S., and Hatzoglou, M. (2013). ER-stress-induced transcriptional regulation increases protein synthesis leading to cell death. *Nat. Cell Biol.* **15**, 481.

Hashimshony, T., Senderovich, N., Avital, G., Klochender, A., de Leeuw, Y., Anavy, L., Gennert, D., Li, S., Livak, K.J., and Rozenblatt-Rosen, O. (2016). CEL-Seq2: sensitive highly-multiplexed single-cell RNA-Seq. *Genome Biol.* **17**, 77.

Heinz, S., Benner, C., Spann, N., Bertolino, E., Lin, Y.C., Laslo, P., Cheng, J.X., Murre, C., Singh, H., and Glass, C.K. (2010). Simple combinations of lineage-determining transcription factors prime cis-regulatory elements required for macrophage and B cell identities. *Mol. Cell* **38**, 576–589.

Immel, T.a., Groth, U., and Huhn, T. (2010). Cytotoxic titanium salan complexes: surprising interaction of salan and alkoxy ligands. *Chem. A. Eur. J.* **16**, 2775–2789.

Immel, T.A., Groth, U., Huhn, T., and Öhlschläger, P. (2011). Titanium salan complexes displays strong antitumor properties in Vitro and in Vivo in mice. *PLoS One* **6**, e17869.

Immel, T.A., Gruzke, M., Spae, A.-K., Groth, U., Hlschlaer, P., and Huhn, T. (2012). Synthesis and X-ray structure analysis of a heptacoordinate titanium(IV)-bis-chelate with enhanced in vivo antitumor efficacy. *Chem. Commun.* **48**, 5790–5792.

Jamieson, E.R., and Lippard, S.J. (1999). Structure, recognition, and processing of cisplatin–DNA adducts. *Chem. Rev.* **99**, 2467–2498.

Jovanović, K.K., Tanić, M., Ivanović, I., Gligorijević, N., Dojčinović, B.P., and Radulović, S. (2016). Cell cycle, apoptosis, cellular uptake and whole-transcriptome microarray gene expression analysis of HeLa cells treated with a ruthenium (II)-arene complex with an isoquinoline-3-carboxylic acid ligand. *J. Inorg. Biochem.* **163**, 362–373.

Kawajiri, K., Nakachi, K.I., zue Imai, K., Watanabe, J., and Hayashi, S. (1993). The CYP1A1 gene and cancer susceptibility. *Crit. Rev. Oncol. Hematol.* **14**, 77–87.

Keppler, B.K., Friesen, C., Moritz, H.G., Vongerichten, H., and Vogel, E. (1991). Tumor-inhibiting bis(β -Diketonato) metal complexes. Budotitane, cis-diethoxybis(1-phenylbutane-1,3-dionato)titanium(IV). In *Bioinorganic Chemistry* (Springer Berlin Heidelberg), pp. 97–127.

Khazaei, S., Esa, N.M., Ramachandran, V., Hamid, R.A., Pandurangan, A.K., Etemad, A., and Ismail, P. (2017). In vitro antiproliferative and apoptosis inducing effect of Allium atroviolaceum bulb extract on breast, cervical, and liver cancer cells. *Front. Pharmacol.* **8**, 5.

- Koepf-Maier, P., and Koepf, H. (1987). Non-platinum group metal antitumor agents. History, current status, and perspectives. *Chem. Rev.* **87**, 1137–1152.
- Komeda, S., and Casini, A. (2012). Next-generation anticancer metallodrugs. *Curr. Top. Med. Chem.* **12**, 219–235.
- Köpf, H., and Köpf-Maier, P. (1979). Titanocene dichloride—the first metallocene with cancerostatic activity. *Angew. Chem. Int. Ed.* **18**, 477–478.
- Kurosaki, T., Maeda, A., Ishiai, M., Hashimoto, A., Inabe, K., and Takata, M. (2000). Regulation of the phospholipase C-gamma2 pathway in B cells. *Immunol. Rev.* **176**, 19–29.
- Loza-Rosas, S.A., Saxena, M., Delgado, Y., Gaur, K., Pandrala, M., and Tinoco, A.D. (2017). A ubiquitous metal, difficult to track: towards an understanding of the regulation of titanium(IV) in humans. *Metallomics* **9**, 346–356.
- Manna, C.M., Braitbard, O., Weiss, E., Hochman, J., and Tshuva, E.Y. (2012). Cytotoxic salan-titanium(IV) complexes: high activity toward a range of sensitive and drug-resistant cell lines, and mechanistic insights. *ChemMedChem* **7**, 703–708.
- Manohari Abeyasinghe, P., and Harding, M.M. (2007). Antitumor bis(cyclopentadienyl) metal complexes: titanocene and molybdocene dichloride and derivatives. *Dalt. Trans.* **32**, 3474–3482.
- Meier-Menches, S.M., Gerner, C., Berger, W., Hartinger, C.G., and Keppler, B.K. (2018). Structure–activity relationships for ruthenium and osmium anticancer agents—towards clinical development. *Chem. Soc. Rev.* **47**, 909–928.
- Meker, S., Margulis-Goshen, K., Weiss, E., Magdassi, S., and Tshuva, E.Y. (2012). High antitumor activity of highly resistant salan-titanium(IV) complexes in nanoparticles: an identified active species. *Angew. Chem. Int. Ed.* **51**, 10515–10517.
- Meker, S., Margulis-Goshen, K., Weiss, E., Braitbard, O., Hochman, J., Magdassi, S., and Tshuva, E.Y. (2014). Anti-proliferative activity of nano-formulated phenolato titanium(IV) complexes against cancer cells. *ChemMedChem* **9**, 1294–1298.
- Meker, S., Braitbard, O., Margulis-Goshen, K., Magdassi, S., Hochman, J., and Tshuva, E.Y. (2015). Highly stable tetra-phenolato titanium(IV) agent formulated into nanoparticles demonstrates anti-tumoral activity and selectivity. *Molecules* **20**, 18526–18538.
- Meker, S., Braitbard, O., Hall, M.D., Hochman, J., and Tshuva, E.Y. (2016). Specific design of titanium(IV) phenolato chelates yields stable and accessible, effective and selective anticancer agents. *Chem. Eur. J.* **22**, 9986–9995.
- Meléndez, E. (2002). Titanium complexes in cancer treatment. *Crit. Rev. Oncol.* **42**, 309–315.
- Meng, A.X., Jalali, F., Cuddihy, A., Chan, N., Bindra, R.S., Glazer, P.M., and Bristow, R.G. (2005). Hypoxia down-regulates DNA double strand break repair gene expression in prostate cancer cells. *Radiother. Oncol.* **76**, 168–176.
- Miller, M., and Tshuva, E.Y. (2018). Synthesis of pure enantiomers of titanium (IV) complexes with chiral diaminobis (phenolato) ligands and their biological reactivity. *Sci. Rep.* **8**, 9705.
- Miller, M., Braitbard, O., Hochman, J., and Tshuva, E.Y. (2016). Insights into molecular mechanism of action of salan titanium(IV) complex with in vitro and in vivo anticancer activity. *J. Inorg. Biochem.* **163**, 250–257.
- Mjos, K.D., and Orvig, C. (2014). Metallodrugs in medicinal inorganic chemistry. *Chem. Rev.* **114**, 4540–4563.
- Nagy, Z., Riss, A., Romier, C., le Guezennec, X., Dongre, A.R., Orpinell, M., Han, J., Stunnenberg, H., and Tora, L. (2009). The human SPT20-containing SAGA complex plays a direct role in the regulation of endoplasmic reticulum stress-induced genes. *Mol. Cell. Biol.* **29**, 1649–1660.
- Ott, I., and Gust, R. (2007). Non platinum metal complexes as anti-cancer drugs. *Arch. Pharm. (Weinheim)* **340**, 117–126.
- Pereira, E.R., Frudd, K., Awad, W., and Hendershot, L.M. (2014). Endoplasmic reticulum (ER) stress and hypoxia response pathways interact to potentiate hypoxia-inducible factor 1 (HIF-1) transcriptional activity on targets like vascular endothelial growth factor (VEGF). *J. Biol. Chem.* **289**, 3352–3364.
- Peri, D., Meker, S., Shavit, M., and Tshuva, E.Y. (2009). Synthesis, characterization, cytotoxicity, and hydrolytic behavior of C2- and C1-symmetrical TiIV complexes of tetradentate diamine bis(phenolato) ligands: a new class of antitumor agents. *Chem. A Eur. J.* **15**, 2403–2415.
- Peri, D., Manna, C.M., Shavit, M., and Tshuva, E.Y. (2011a). TiIV complexes of branched diamine bis(phenolato) ligands: hydrolysis and cytotoxicity. *Eur. J. Inorg. Chem.* **31**, 4896–4900.
- Peri, D., Meker, S., Manna, C.M., and Tshuva, E.Y. (2011b). Different ortho and para electronic effects on hydrolysis and cytotoxicity of diamino bis(Phenolato) “Salan” Ti(IV) complexes. *Inorg. Chem.* **50**, 1030–1038.
- Riddell, I.A., and Lippard, S.J. (2018). Cisplatin and oxalipatin: our current understanding of their actions. *Met. Ions Life Sci.* **18**, 1–42.
- Rustum, Y.M., Harstrick, A., Cao, S., Vanhoefler, U., Yin, M.-B., Wilke, H., and Seeber, S. (1997). Thymidylate synthase inhibitors in cancer therapy: direct and indirect inhibitors. *J. Clin. Oncol.* **15**, 389–400.
- Rzyski, T., Milani, M., Singleton, D.C., and Harris, A.L. (2009). Role of ATF4 in regulation of autophagy and resistance to drugs and hypoxia. *Cell Cycle* **8**, 3838–3847.
- Schur, J., Manna, C.M., Deally, A., Koester, R.W., Tacke, M., Tshuva, E.Y., and Ott, I. (2013). A comparative chemical-biological evaluation of titanium(IV) complexes with a salan or cyclopentadienyl ligand. *Chem. Commun.* **49**, 4785–4787.
- Sharma, K.L., Agarwal, A., Misra, S., Kumar, A., Kumar, V., and Mittal, B. (2014). Association of genetic variants of xenobiotic and estrogen metabolism pathway (CYP1A1 and CYP1B1) with gallbladder cancer susceptibility. *Tumor Biol.* **35**, 5431–5439.
- Shavit, M., Peri, D., Melman, A., and Tshuva, E.Y. (2007). Antitumor reactivity of non-metallocene titanium complexes of oxygen-based ligands: is ligand lability essential? *J. Biol. Inorg. Chem.* **12**, 825–830.
- Suntharalingam, K., Johnstone, T.C., Bruno, P.M., Lin, W., Hemann, M.T., and Lippard, S.J. (2013). Bidentate ligands on osmium (VI) nitrido complexes control intracellular targeting and cell death pathways. *J. Am. Chem. Soc.* **135**, 14060–14063.
- Suntharalingam, K., Lin, W., Johnstone, T.C., Bruno, P.M., Zheng, Y.-R., Hemann, M.T., and Lippard, S.J. (2014). A breast cancer stem cell-selective, mammospheres-potent osmium (VI) nitrido complex. *J. Am. Chem. Soc.* **136**, 14413–14416.
- Tinoco, A.D., Thomas, H.R., Incarvito, C.D., Saghatelian, A., and Valentine, A.M. (2012). Cytotoxicity of a Ti (IV) compound is independent of serum proteins. *Proc. Natl. Acad. Sci. U S A* **109**, 5016–5021.
- Toney, J.H., and Marks, T.J. (1985). Hydrolysis chemistry of the metallocene dichlorides $M(\eta^5-C_5H_5)_2Cl_2$, $M =$ titanium, vanadium, or zirconium. Aqueous kinetics, equilibria, and mechanistic implications for a new class of antitumor agents. *J. Am. Chem. Soc.* **107**, 947–953.
- Tshuva, E.Y., and Ashenhurst, J.A. (2009). Cytotoxic titanium(IV) complexes: renaissance. *Eur. J. Inorg. Chem.* **2009**, 2203–2218.
- Tshuva, E.Y., and Miller, M. (2018). Coordination complexes of titanium(IV) for anticancer therapy. In *Metallo-Drugs: Development and Action of Anticancer Agents*, pp. 219–249.
- Tshuva, E.Y., and Tzuber, A. (2017). Cytotoxic titanium(IV) complexes of salalene-based ligands. *Eur. J. Inorg. Chem.* **12**, 1695–1705.
- Tzuber, A., and Tshuva, E.Y. (2012). Cytotoxicity and hydrolysis of trans -Ti(IV) complexes of salen ligands: structure-activity relationship studies. *Inorg. Chem.* **51**, 1796–1804.
- Tzuber, A., Melamed-Book, N., and Tshuva, E.Y. (2018). Fluorescent antitumor titanium(IV) salen complexes for cell imaging. *Dalt. Trans.* **47**, 3669–3673.
- Velma, V., Dasari, S.R., and Tchounwou, P.B. (2016). Low doses of cisplatin induce gene alterations, cell cycle arrest, and apoptosis in human promyelocytic leukemia cells. *Biomark. Insights* **11**, 113–121.

Wagner, S., Herrmannová, A., Malík, R., Peclínová, L., and Valášek, L.S. (2014). Functional and biochemical characterization of human eukaryotic translation initiation factor 3 in living cells. *Mol. Cell. Biol.* *34*, 3041–3052.

Wang, D., and Lippard, S.J. (2005). Cellular processing of platinum anticancer drugs. *Nat. Rev. Drug Discov.* *4*, 307.

Wang, H., Zhang, T., Sun, W., Wang, Z., Zuo, D., Zhou, Z., Li, S., Xu, J., Yin, F., and Hua, Y. (2016). Erianin induces G2/M-phase arrest, apoptosis, and autophagy via the ROS/JNK signaling pathway in human osteosarcoma cells in vitro and in vivo. *Cell Death Dis.* *7*, e2247.

Yang, X.-L., and Wang, A.H.-J. (1999). Structural studies of atom-specific anticancer

drugs acting on DNA. *Pharmacol. Ther.* *83*, 181–215.

Zogzas, C.E., and Mukhopadhyay, S. (2018). Putative metal binding site in the transmembrane domain of the manganese transporter SLC30A10 is different from that of related zinc transporters. *Metallomics* *10*, 1053–1064.

iScience, Volume 23

Supplemental Information

**Titanium Tackles the Endoplasmic
Reticulum: A First Genomic Study
on a Titanium Anticancer Metallodrug**

Maya Miller, Anna Mellul, Maya Braun, Dana Sherill-Rofe, Emiliano Cohen, Zohar Shpilt, Irene Unterman, Ori Braitbard, Jacob Hochman, Edit Y. Tshuva, and Yuval Tabach

Supplemental Information

PhenolaTi

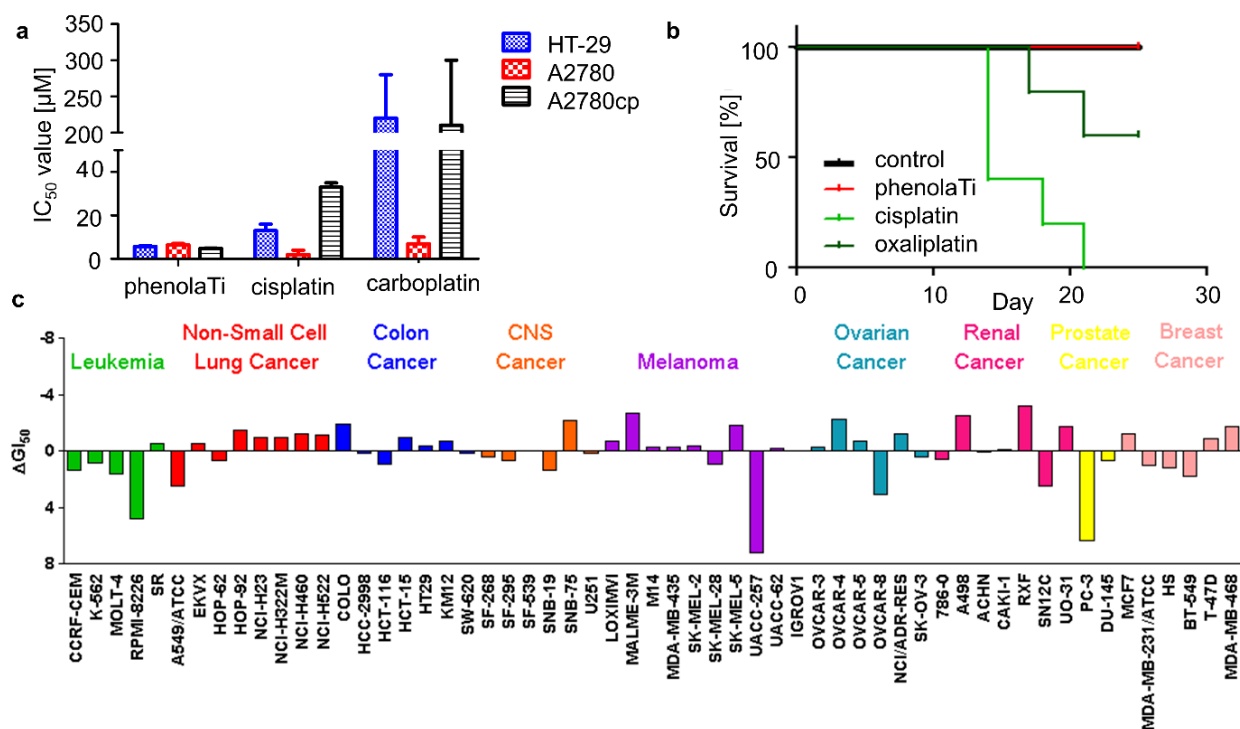


Figure S1: PhenolaTi is a lead anticancer metallodrug. Related to Scheme 1. (a) Relative IC_{50} values (μM) towards HT-29, A2780 and A2780cp (cisplatin resistant) human cancer cell lines of phenolaTi, cisplatin and carboplatin (Meker et al., 2016) (after 72 hours of incubation) (b) *In vivo* effect of phenolaTi (1.6 mg/kg), cisplatin (5 mg/kg), and oxaliplatin (5 mg/kg) on survival of Balb/c mice (Ganot et al., 2018) (c) Relative sensitivity of ca. 60 human cancer cell lines of the NCI-60 panel to phenolaTi, GI_{50} 4.6 ± 2 μM (equivalent to IC_{50} ; the equation for GI_{50} derivatization is given in following reference (Meker et al., 2016)).

In vitro cytotoxicity

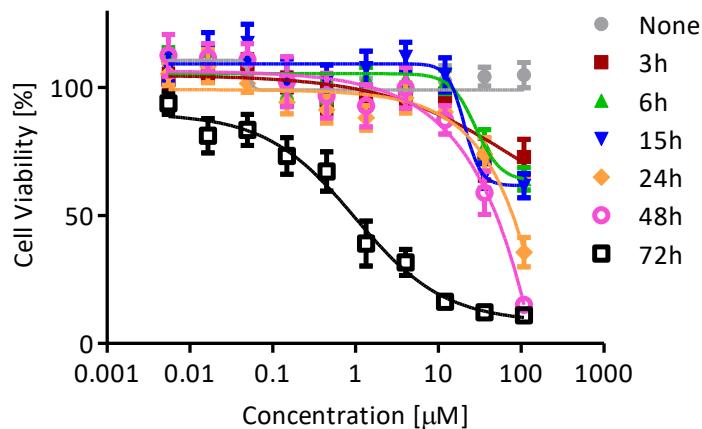


Figure S2: Cytotoxicity curves of phenolaTi. Related to Figure 1. Viability curves of phenolaTi toward human MCF7 breast adenocarcinoma cells using the methylthiazolyldiphenyl-tetrazolium bromide (MTT) (Ganot et al., 2013) assay following different incubation times. Relative IC_{50} at 72 hours is $0.65 \pm 0.30 \mu\text{M}$.

MCF7 cells were selected due to their relative sensitivity to phenolaTi, as deduced from the results previously published on the reactivity toward the NCI-60 panel of the NIH (Meker et al., 2016). The results depict that MCF7 cells were most sensitive to phenolaTi after 72 hours, although some activity was also observed following shorter incubation times. No evident toxicity was observed for at least 6 hours, indicating an anti-neoplastic effect executed through regulated molecular signaling pathways.

Flow cytometry

Cell cycle and apoptosis distribution

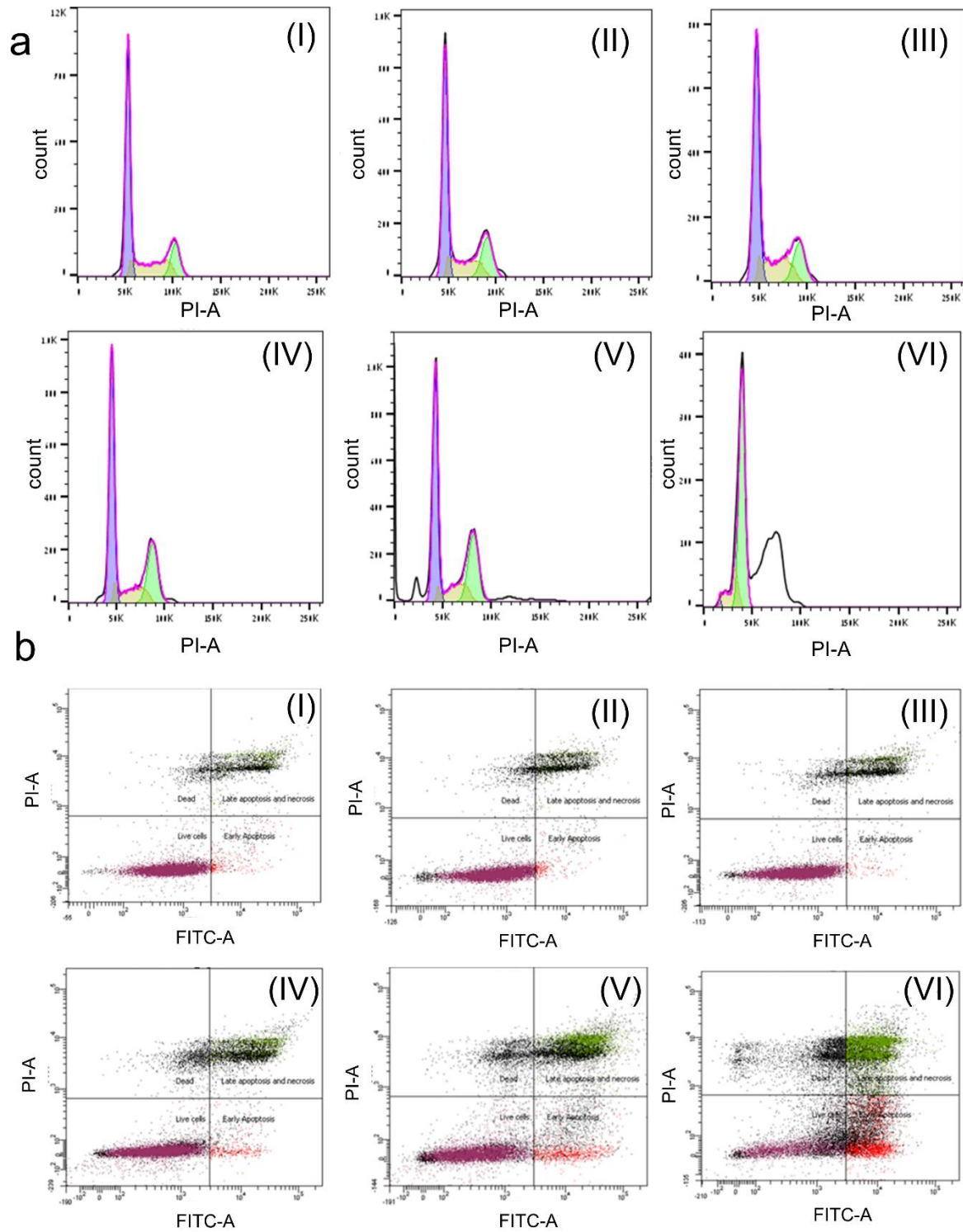


Figure S3: MCF7 cells undergo changes in response to phenolTi treatment. Related to Figure 2.; (a) Cell cycle distribution following a 54 μM at different time points: (I) control (0 hours- untreated); and after (II) 3 (III) 6 (IV) 15 (V) 24 (VI) 48 hours of incubation (showing one of three repeats). (b) Time dependent effect of phenolTi at 54 μM on apoptosis in MCF7 cancer cells, as recorded using flow cytometry, (I) control (0

hours- untreated); and after (II) 3 (III) 6 (IV) 15 (V) 24 (VI) 48 hours of incubation (showing one of three repeats).

Short term effect (3-15 h) of phenolaTi

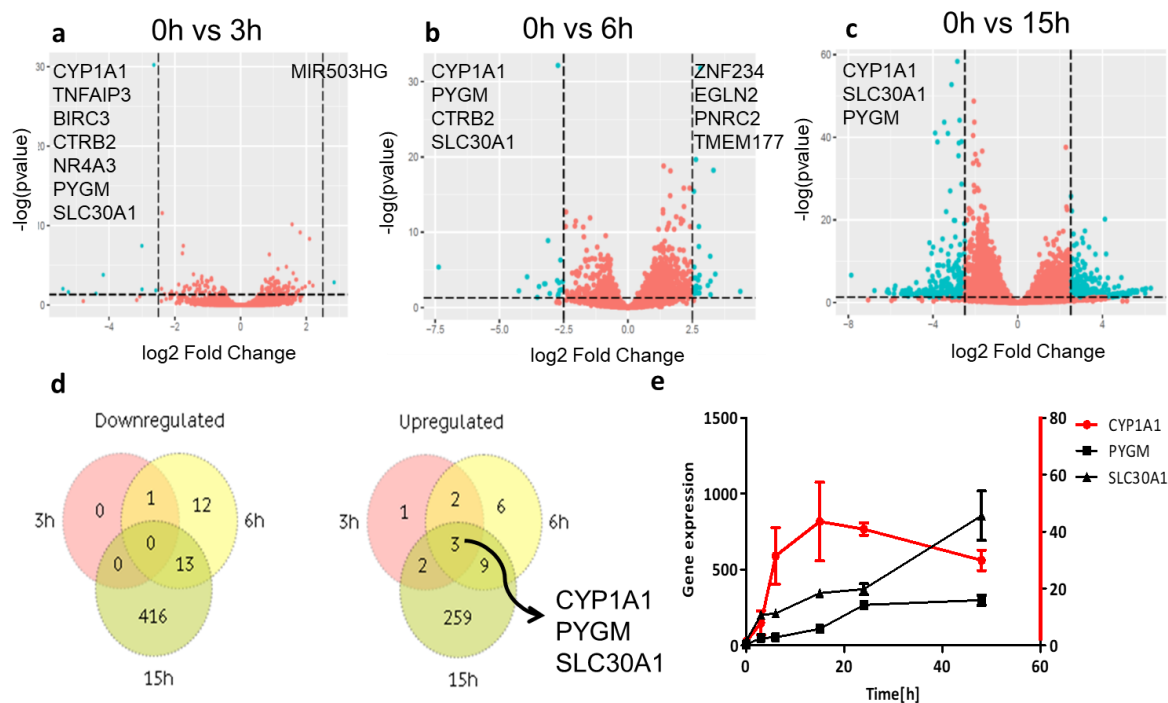


Figure S4: Short term changes in genes expressions after treatment with phenolaTi. Related to Figure 2. (a-c) The volcano plots describe the fold change expression of the genes (x-axis) and the p-value for significant changes in expression (blue dots present significant change, up-left or down-right regulated, between the selected time point and 0- untreated cells) at three time points (a) 3 (b) 6 and (c) 15 hours of exposure relative to control (untreated cells) (d) Venn diagram describes overlap of altered genes at different time points divided into up and down regulated genes (e) Gene expression of CYP1A1, PYGM and SLC30A1 over time.

Nine genes showed significant changes (Q-value < 0.05, and fold change > 2) already within 3 hours of exposure, followed by 46 genes at 6 hours, and subsequently 702 genes after 15 hours of incubation. The most significantly altered gene (p-value 4.7e-35) SLC30A1 is associated to cation transmembrane transporters and calcium channel inhibitor activity. Interestingly, upregulations of this and related genes are involved in zinc efflux localized in the endoplasmic reticulum membrane (Barresi et al., 2018). Another significantly upregulated gene is PYGM, an enzyme in carbohydrate metabolism. Of the 46 genes changed within 6 hours, 19 genes were upregulated, and 27 genes were downregulated (Fig. S4a-e); among the downregulated genes, EGLN2 (p-value 4.66e-6) is involved in oxygen sensing related to hypoxia tolerance. Additional downregulated genes are PNRC2 (p-value 5.6e-24) associated with energy balance/storage, and TMEM177 (p-value 2.2e-22) – a mitochondrial respiratory chain complex assembly factor. This gene signature further supports the effect on mitochondria previously observed for related Ti phenolato compounds, accumulated in the mitochondria organelle (Schur et al., 2013). Examining the 702 genes that were changed at 15 hours, 272 were upregulated and 430 downregulated. The downregulated genes relate to cell cycle checkpoints such as CDC23 gene, and DNA damage such as BRCA1 gene. The upregulated genes relate to cellular response to metal ions such as CYP1A1.

CYP1A1 is a member of cytochrome p450 superfamily enzymes, which are involved in drug metabolism and monooxygenase reactions (from NAD(P)H). These proteins are localized mainly in the inner membrane of the mitochondria or the endoplasmic reticulum and are associated with cancer susceptibility (Agúndez, 2004; Brignac-Huber et al., 2016; name Kawajiri et al., 1993; Sharma et al., 2014). CYP1A1 together with PYGM (see above) and SLC30A1 genes (Fig. S4e) are immediately upregulated in response to phenolaTi, stay highly expressed through the short times (3,6,15 hours). PYGM relates to phosphorylase activity in glycogen metabolism (Smutna et al., 2014) and SLC30A1 relates to cellular

metal transport (Guo and Cousins, 2009). Interestingly, two out of three proteins (SLC30A1 and CYP1A1) are functionally related to the endoplasmic reticulum.

Gene Set Enrichment Analysis (Liberzon et al., 2011; Subramanian et al., 2005)

Cluster I

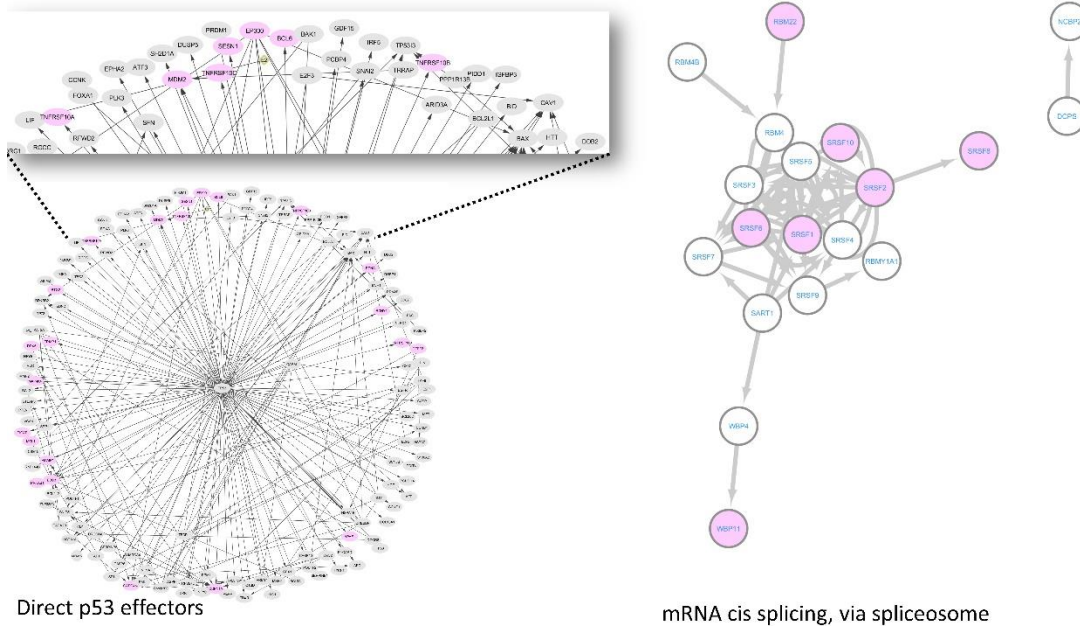
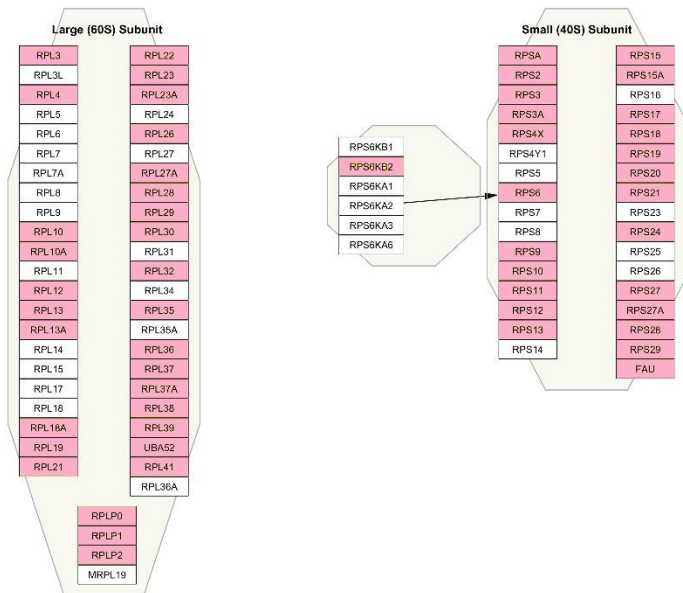


Figure S5: Gene set enrichment analysis using Molecular Signatures Database (MSigDB) for gene expressed in Cluster I. Related to Figure 3. Two representative pathways and our corresponding expressed genes (pink): direct p53 effectors and mRNA cis splicing, via spliceosome pathways.

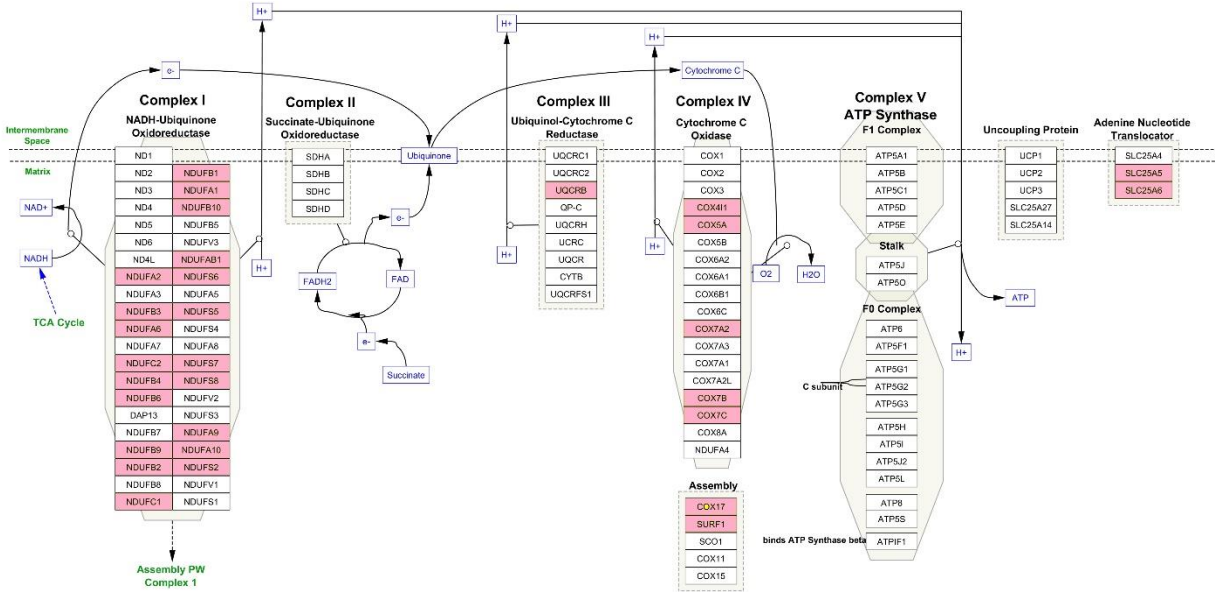
Cluster II



Cytoplasmic Ribosomal Proteins

Figure S6: Gene set enrichment analysis using Molecular Signatures Database (MSigDB) for gene expressed in Cluster II. Related to Figure 3. One representative pathway and our corresponding expressed genes (pink): cytoplasmic ribosomal proteins pathway.

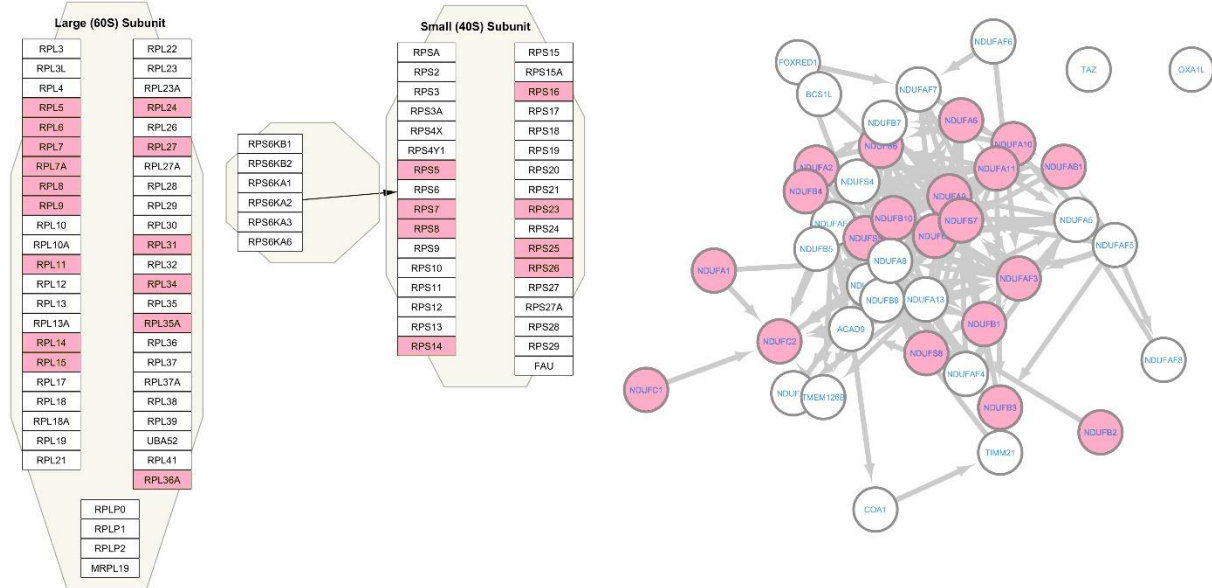
Cluster III



Electron Transport Chain (OXPHOS system in mitochondria)

Figure S7: Gene set enrichment analysis using Molecular Signatures Database (MSigDB) for gene expressed in Cluster III. Related to Figure 3. One representative pathway and our corresponding expressed genes (pink): electron transport chain (OXPHOS system in mitochondria) pathway.

Cluster III

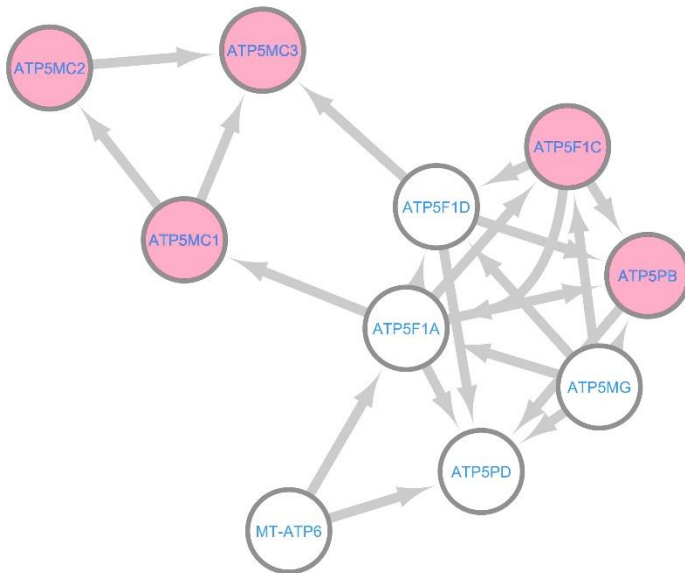


Cytoplasmic Ribosomal Proteins

Mitochondrial respiratory chain complex I

Figure S8: Gene set enrichment analysis using Molecular Signatures Database (MSigDB) for gene expressed in Cluster III. Related to Figure 3. Two additional representative pathways and our corresponding expressed genes (pink): cytoplasmic ribosomal proteins and mitochondrial respiratory chain complex 1 pathways.

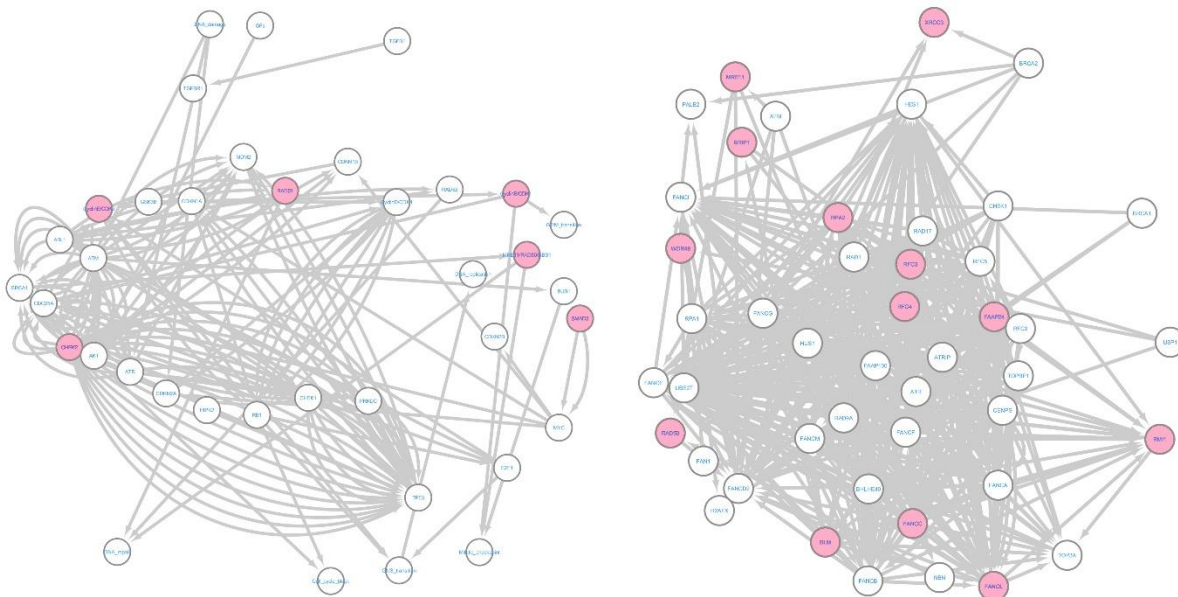
Cluster IV



ATP synthesis coupled proton transport

Figure S9: Gene set enrichment analysis using Molecular Signatures Database (MSigDB) for gene expressed in Cluster IV. Related to Figure 3. One representative pathway and our corresponding expressed genes (pink): ATP synthesis coupled proton transport pathway.

Cluster V



Cell cycle G2M phase transition

Fanconi anemia pathway

Figure S10: Gene set enrichment analysis using Molecular Signatures Database (MSigDB) for gene expressed in Cluster V. Related to Figure 3. Two representative pathways and our corresponding expressed genes (pink): cell cycle G2/M phase transition and Fanoconi anemia pathways.

Analysis of pathway related genes: PhenolTi causes changes in hypoxia and endoplasmic reticulum related genes

Endoplasmic reticulum related genes

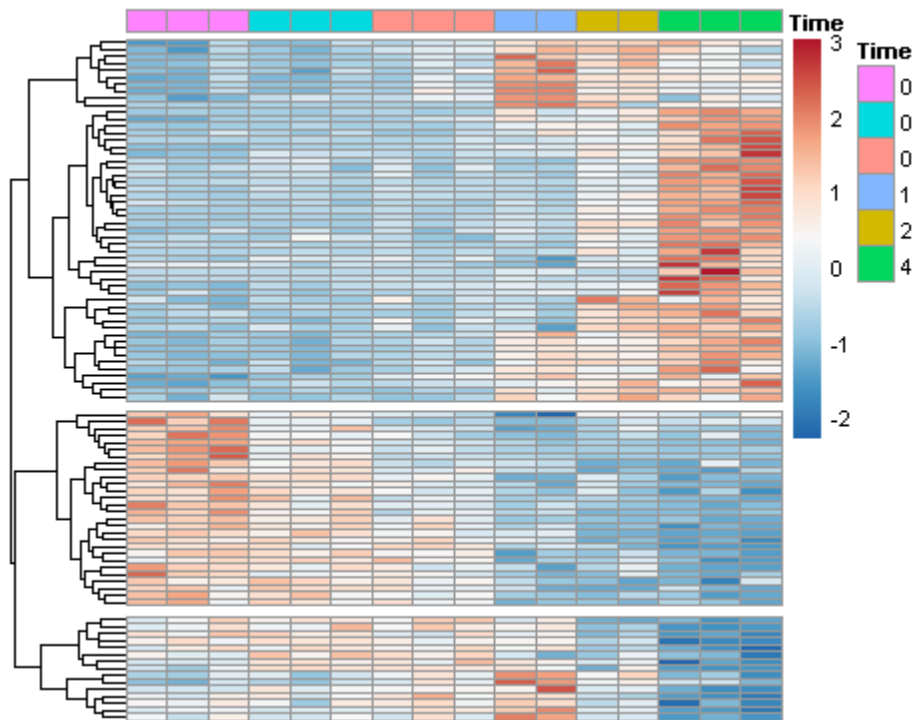


Figure S11: Changes in expression of ER related genes in response to phenolTi in MCF7 cells at 54 μ M. Related to Figure 4. A 95-gene cluster of the total 575 genes previously reported to relate to ER stress (Han et al., 2013); these genes were significantly altered over time in our experiment (p-value < 0.001).

Gene validation- ddPCR

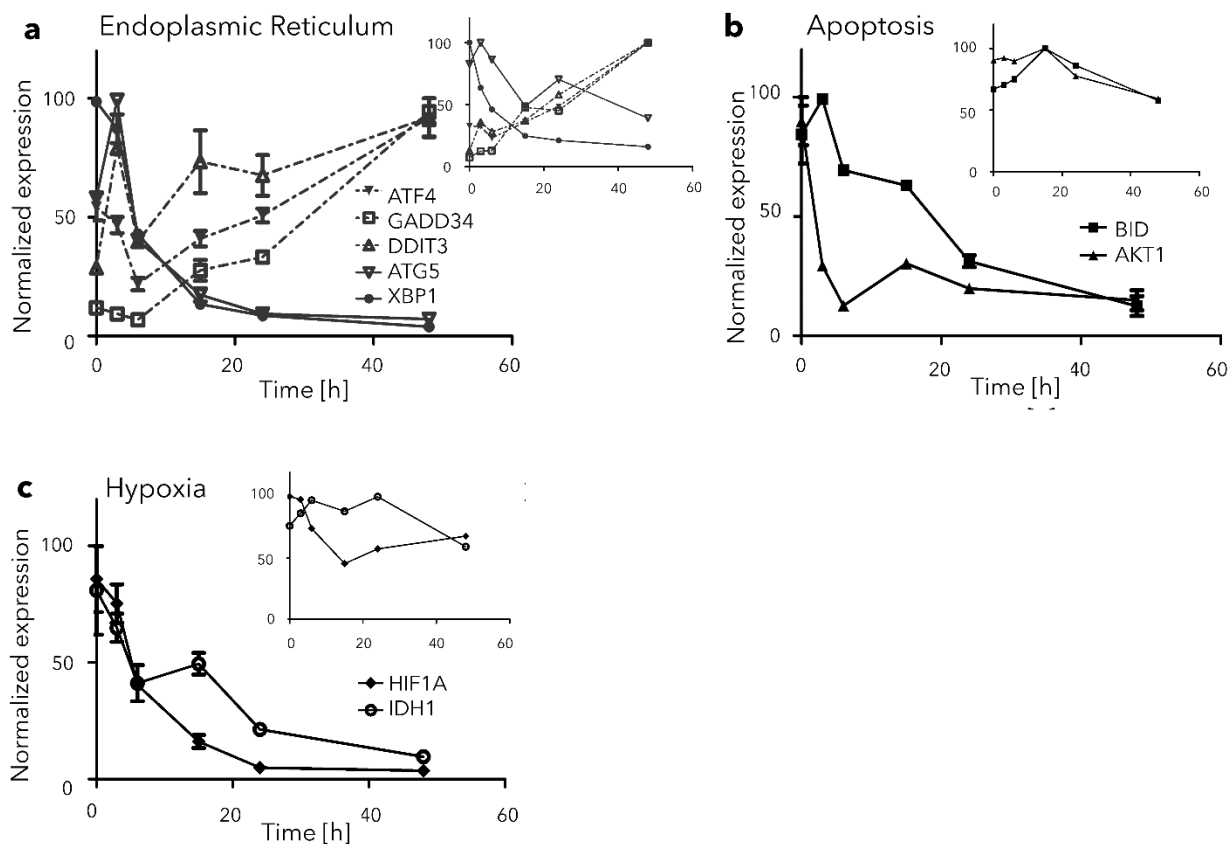


Figure S12: Gene expression alteration in response to phenolTi in MCF7 cells: RNA-seq correlates with ddPCR results. Related to Figure 4. Cells were treated with 54 μ M phenolTi and sequenced in duplicate after 0 (untreated), 3, 6, 15, 24 and 48 hours. Expression analysis included ddPCR. Normalization was performed relative to the maximal expression of each gene. (a) Five representative genes related to endoplasmic reticulum stress are depicted (ATF4, GADD34, DDIT3, ATG5, XBP1). Upper level (minimized graph) expression illustrates the results obtained through RNA-seq of the corresponding genes. (b) Two representative genes, related to apoptosis are depicted (BID, AKT1). Upper level (minimized graph) expression illustrates the results obtained through RNA-seq of the corresponding genes. (c) Two representative genes, related to hypoxia are depicted (HIF1A, IDH1). Upper level (minimized graph) expression illustrates the results obtained through RNA-seq of the corresponding genes for comparison.

Independent p53 cytotoxicity

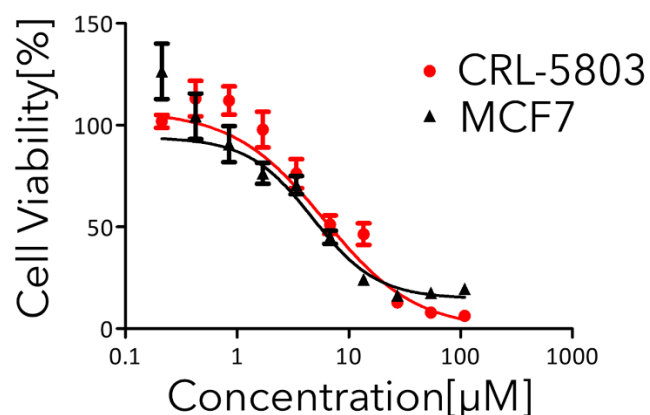


Figure S13: *In vitro* validation assay is independent of p53 cellular status. Related to Figure 5. Cytotoxicity curves of phenolaTi toward human MCF7 and CRL-5803 cancer cells using the MTT assay following 72 hours of incubation, showing similar activity. Relative IC_{50} of phenolaTi on MCF7 and CRL-5803: 4.59 ± 1.78 and 6.66 ± 1.75 μM , respectively.

The cell cycle arrest and altered DNA repair pathways, as well as the apoptotic response, suggest the involvement of TP53. The transcriptomic analysis points to participation of p53 protein in the cellular response to phenolaTi in three main clusters (Fig. 3 cluster (I)/(III)/(V)). Whereas some p53 regulating genes are downregulated (Fig. 3 cluster (V)), such as CHEK2, CDK1 and RAD51, most related genes are upregulated within 15 or 48 hours (Fig. 3 cluster (III)/(I)), among which are GADD45 and BCL6. To measure dependency of the cytotoxic effect of phenolaTi on p53 status, cell viability was compared for two cell lines, based on the methylthiazolyldiphenyl-tetrazolium bromide (MTT) assay (Ganot et al., 2013): MCF7 cells with wild type p53 gene (Wasielewski et al., 2006), and CRL-5803 lung carcinoma p53 null-cell line (Blandino et al., 1999) (Supplemental Fig. S7).

Both cell lines responded similarly to the phenolaTi treatment. This result may suggest a p53 independent mode of action of phenolaTi and may point to an alternative DNA-damage and apoptotic-response pathways, e.g. the AKT pathway (Roos et al., 2016). This observation agrees with the cytotoxic effect of phenolaTi on all lines in the NCI-60 panel, comprising both wild type and mutated TP53 cell lines (Supplemental Fig. S1c), as well as with previous reports suggesting upregulation of p53 amounts in response to Ti(IV) phenolato-based compounds (Miller et al., 2016).

Transparent Methods

General: Complex phenolaTi was synthesized according to published procedures (Meker et al., 2016). In all experiments, the compounds were first dissolved in DMSO and then diluted in medium as appropriate.

Cell lines and culture conditions: All experiments were conducted on human MCF7 (breast adenocarcinoma, genetic characterization can be found at <https://www.atcc.org/products/all/HTB-22.aspx#specifications>, or CRL-5803 (NCI-H1299; lung carcinoma) cells obtained from American Type Culture Collection (ATCC) Inc. Cells were grown in 75-cm² culture flasks as adherent monolayer cultures in Dulbecco's Modified Eagle's Medium (DMEM) or Roswell Park Memorial Institute (RPMI) 1640 medium, respectively, supplemented with 10% fetal bovine serum, 1% L-glutamine and 1% penicillin/streptomycin (Biological Industries).

Cytotoxicity: Cells were grown in 96-well plate at density of ~9,000 cells per well, allowed to attach overnight, and incubated for 0 (untreated), 3, 6, 15, 24, 48 and 72 hours with phenolaTi. Then, the MTT assay was applied as previously described (Ganot et al., 2013). Each measurement was repeated at least 3×3 times, namely, three repeats per plate, all repeated three times on different days (9 repeats altogether). Relative IC₅₀ values with standard error of means were determined by a nonlinear regression of a variable slope (four parameters) model by the Graph Pad Prism5.0 program.

Experiments conducted on CRL-5803 cells were measured after 72 hours of incubation, according to a published procedure (Ganot et al., 2013).

Experiments conducted with salubrinal (purchased from Sigma) included 70 μM substrate added to the cells, 12 hours prior to addition of phenolaTi, based on previous studies suggesting rapid cellular penetration of phenolaTi (Meker et al., 2016).

Cell cycle analysis: Cells were cultured in a 6-well plate at a density of ~200,000 cells per well and allowed to attach overnight. PhenolaTi was added at a 54 μM concentration and incubated for 0 (untreated)/3/6/15/24/48 hours, such that all samples were harvested at the same time. Cells were trypsinized and medium was added. The samples were then centrifuged at 2,000 RPM for 5 minutes, washed twice with PBS, and fixed at least overnight in a 1:3 PBS to ethanol solution at 4 °C. Cells were then centrifuged at 2,000 RPM for 5 minutes and washed with 0.4 ml PBS. Afterwards, 3.5 μl of RNase A were added, and the cells were incubated for 15 min at 37 °C, stained with propidium iodide at 4 °C for 30 minutes, and analyzed by flow cytometry (Becton-Dickinson Excalibur Fluorescence Activated Cell Sorter) using the FlowJo program (Treestar, San Carlos, CA, USA). Each experiment was conducted at least 3 times on different days.

Annexin V/propidium iodide assay: Apoptosis was measured using the Annexin V FITC Apoptosis detection kit (Calbiochem). Cells were cultured in a 6-well plate at a density of ~300,000 cells per well and allowed to attach overnight. PhenolaTi was added at a 54 μM concentration and incubated for 0 (untreated)/3/6/15/24/48 hours, so that all samples were harvested at the same time. All procedures were conducted according to the manufacturer's instructions. The samples were analyzed by flow cytometry (Becton-Dickinson Excalibur Fluorescence Activated Cell Sorter).

Microscopy: Cells were cultured in a 6-well plate at a density of ~300,000 cells per well and allowed to attach overnight. The next day, phenolaTi (54 μM) or DMSO (0.5%) were added and the cells were incubated for 72 hours. The cell response was recorded every 15 minutes for 72 hours by Nikon eclipse-Ti.

RNaseq analysis: RNA was purified from MCF7 cells treated with 54 μM phenolaTi for different incubation periods (0-untreated/3/6/15/24/48 hours), in three biological replicates (one sample each for 15 and 24 incubation time points were omitted) and sequenced using the Cel-Seq2 method (Hashimshony et al., 2016). The results were analyzed as follows: 1) The pair-end samples were demultiplexed as previously published (Hashimshony et al., 2016); 2) Adapters were trimmed by cutadapt; 3) The reads were mapped to the human genome version GRCh38 using STAR (Dobin et al., 2013); 4) The reads were counted by HTseq-count (Anders et al., 2015); 5) The count matrix was normalized to the size of all the libraries analyzed; 6) The z-score of the normalized data was calculated. A one-way ANOVA test was employed to identify the genes that had a similar expression within the biological replicates but the highest

level of variation with the other samples. The results were ordered by their p-values and the top 5,000 genes were selected for in-depth analysis. These genes were clustered into 5 groups according to their expression levels. These groups were analyzed with HOMER (Heinz et al., 2010) in order to find common transcription factors.

ddPCR: The same samples used for RNA-sequencing were used for the ddPCR procedure, employed on the selected genes. Reverse transcription was performed using a cDNA reverse transcript kit (iScript™ cDNA Synthesis kit; Bio-Rad), according to manufacturer's instructions. The mRNA expression levels were measured by using QX200™ Bio-Rad digital droplet PCR. Primers for each gene were purchased from Sigma Aldrich accordingly:

ATF4 (F: AGGAGGAAGACACCCCTTCA, R: ATCGTAAGGTTTGGGACGGG), GADD34 (F: CTGGCTGGTGGGAAGCAGTAA, R: TATGGGGGATTGCCAGAGGA), DDIT3 (F: TTCTCTGGCTTGGCTGACTG, R: TCCTCCTCTTCCTCCTGAGC), ATG5 (F: TTTGGTGGAGGCAACCTGAC, R: CCAGCCCAGTTGCCTTATCT), XBP1 (F: TGACATCCAGCAGTCCAAGG, R: GCAAGCCAGGATGCCAAAAA), BID (F: CCAGAACCTACGCACCTACG, R: ACCACATCGAGCTTTAGCCA), AKT1 (F: GGACAAGGACGGGCACATTA, R: CGACCGCACATCATCTCGTA), HIF1A (F: GGCAGCAACGACACAGAAAC, R: TTTTCGTTGGGTGAGGGGAG) and IDH1 (F: ACGGAACCCAAAAGGTGACA, R: GCCAACCCCTTAGACAGAGCC).

Polymerase chain reaction (PCR): MCF7 cells were grown in 75-cm² cell culture flasks (Nunc™, Thermo Fisher Scientific). About 3x10⁶ cells were trypsinized and DNA was extracted and purified using NucleoSpin® Tissue (Macherey-Nagel), according to the manufacturer's instructions. The DNA concentration was 60 ng/μl. The DNA concentration was set to 0.4 ng/μl, correlating to 20,000 cells. For the PCR protocol, the REDTaq® ReadyMix™ PCR reaction mix (R2523, Sigma Aldrich) was used. The actin gene was used as the housekeeping gene for evaluation of possible interaction. Primers (F:AGACTCTGTCTGGCAGTTG, R: CAGCTGGTAAGGGGGACTTG) were purchased from Sigma. Cisplatin, doxorubicin and 5-fluorouracil were purchased from Sigma. The concentration used for all tested compounds was 27 and 54 μM, in duplicates; all repeated at least three times.

Immunoblotting assay: Cells were cultured in 6-well plate at density of ~200,000 cells per well and allowed to attach overnight. PhenolTi was added at 54 μM and the wells were incubated for 16 and 24 hours. Cell protein extracts were obtained by adding Laemmli sample buffer (Bio-Rad, #161-0747) supplemented with 10% β-mercaptoethanol. About 40 μg of total protein (determined by BCA method) was loaded on gradient 4-20% Mini-Protean® TGX Stain-Free protein gel (Bio-Rad), in tris-glycine-SDS running buffer, resolved at 25 mA (per gel) and electroblotted to nitrocellulose or activated polyvinylidene fluoride (PVDF) membrane at Trans-Blot Turbo Transfer system (Bio-Rad). The membranes were blocked with 3% non-fat milk solution in Tris buffered saline and Tween 20 (TBST) for 1 hour at room temperature. Membranes were incubated for overnight at 4 °C with either anti- PERK (1:400, #3192, Cell Signaling), GAPDH (1:400, ab181602, EPR16891, ABCAM), p-EIF2α (1:400, ab32157, E90, ABCAM), ATF4 (1:400, ab184909, EPR18111, ABCAM), p-IRE1 (1:400, ab124945, EPR5253, ABCAM), primary antibody diluted in blocking solution. Membranes were washed and then incubated with peroxidase conjugated secondary antibodies (1:10,000, Sigma) diluted in blocking solution for 1 hour at room temperature. The membranes were washed with TBST and proteins were visualized using enhanced chemiluminescence (ECL) solution (Bio-Rad) using Gel Doc™ imaging system (Bio-Rad).

Gene expression (qPCR): Total RNA was extracted from MCF7 cells similarly to RNA-seq analysis. Reverse transcription was performed using iScript cDNA synthesis kit (Bio-Rad), and mRNA expression levels were measured with qPCR. SYBR-Green (Bio-Rad, USA) was used in a CFX-384 Real-Time PCR system (Bio-Rad). Data were analyzed using the ΔΔCt method. Relative quantities of gene transcripts were normalized to actin (same primer as in PCR section). Primers for the spliced variant of XBP1 protein were specifically designed on the 26 base gap differentiated between the long and spliced variants, using the NCBI Primer Blast (F: CTGAGTCCGCAGCAGGTGCAG, R: GAGATACCCAGCTCCGGAACG).

Supplemental References:

Agúndez, J.A.G. (2004). Cytochrome P450 gene polymorphism and cancer. *Curr. Drug Metab.* 5, 211–224.

Anders, S., Pyl, P.T., and Huber, W. (2015). HTSeq—a Python framework to work with high-throughput sequencing data. *Bioinformatics* 31, 166–169.

Barresi, V., Valenti, G., Spampinato, G., Musso, N., Castorina, S., Rizzarelli, E., and Condorelli, D.F. (2018). Transcriptome analysis reveals an altered expression profile of zinc transporters in colorectal cancer. *J. Cell. Biochem.* 119, 9707–9719.

Blandino, G., Levine, A.J., and Oren, M. (1999). Mutant p53 gain of function: differential effects of different p53 mutants on resistance of cultured cells to chemotherapy. *Oncogene* 18, 477.

Brignac-Huber, L.M., Park, J.W., Reed, J.R., and Backes, W.L. (2016). Cytochrome P450 organization and function are modulated by endoplasmic reticulum phospholipid heterogeneity. *Drug Metab. Dispos.* 44, 1859–1866.

Dobin, A., Davis, C.A., Schlesinger, F., Drenkow, J., Zaleski, C., Jha, S., Batut, P., Chaisson, M., and Gingeras, T.R. (2013). STAR: ultrafast universal RNA-seq aligner. *Bioinformatics* 29, 15–21.

Ganot, N., Meker, S., Reytman, L., Tzuber, A., and Tshuva, E.Y. (2013). Anticancer Metal Complexes: Synthesis and Cytotoxicity Evaluation by the MTT Assay. *J. Vis. Exp.* e50767.

Ganot, N., Braitbard, O., Gammal, A., Tam, J., Hochman, J., and Tshuva, E.Y. (2018). In Vivo Anticancer Activity of a Nontoxic Inert Phenolato Titanium Complex: High Efficacy on Solid Tumors Alone and Combined with Platinum Drugs. *ChemMedChem* 13, 2290–2296.

Guo, L., and Cousins, R.J. (2009). Zinc-regulated ZnT1 (SLC30A1) and Glucocorticoid-regulated ZnT2 (SLC30A2) Influence Zinc Efflux from Pancreatic Acinar Cells.

Han, J., Back, S.H., Hur, J., Lin, Y.-H., Gildersleeve, R., Shan, J., Yuan, C.L., Krokowski, D., Wang, S., and Hatzoglou, M. (2013). ER-stress-induced transcriptional regulation increases protein synthesis leading to cell death. *Nat. Cell Biol.* 15, 481.

Hashimshony, T., Senderovich, N., Avital, G., Klochendler, A., de Leeuw, Y., Anavy, L., Gennert, D., Li, S., Livak, K.J., and Rozenblatt-Rosen, O. (2016). CEL-Seq2: sensitive highly-multiplexed single-cell RNA-Seq. *Genome Biol.* 17, 77.

Heinz, S., Benner, C., Spann, N., Bertolino, E., Lin, Y.C., Laslo, P., Cheng, J.X., Murre, C., Singh, H., and Glass, C.K. (2010). Simple combinations of lineage-determining transcription factors prime cis-regulatory elements required for macrophage and B cell identities. *Mol. Cell* 38, 576–589.

Liberzon, A., Subramanian, A., Pinchback, R., Thorvaldsdóttir, H., Tamayo, P., and Mesirov, J.P. (2011). Molecular signatures database (MSigDB) 3.0. *Bioinformatics* 27, 1739–1740.

Meker, S., Braitbard, O., Hall, M.D., Hochman, J., and Tshuva, E.Y. (2016). Specific Design of Titanium(IV) Phenolato Chelates Yields Stable and Accessible, Effective and Selective Anticancer Agents. *Chem. Eur. J.* 22, 9986–9995.

Miller, M., Braitbard, O., Hochman, J., and Tshuva, E.Y. (2016). Insights into molecular mechanism of action of salan titanium(IV) complex with in vitro and in vivo anticancer activity. *J. Inorg. Biochem.* 163, 250–257.

name Kawajiri, K., Nakachi, K.I., zue Imai, K., Watanabe, J., and Hayashi, S. (1993). The CYP1A1 gene and cancer susceptibility. *Crit. Rev. Oncol. Hematol.* 14, 77–87.

Roos, W.P., Thomas, A.D., and Kaina, B. (2016). DNA damage and the balance between survival and death in cancer biology. *Nat. Rev. Cancer* 16, 20.

Schur, J., Manna, C.M., Deally, A., Koester, R.W., Tacke, M., Tshuva, E.Y., and Ott, I. (2013). A comparative chemical-biological evaluation of titanium(IV) complexes with a salan or cyclopentadienyl ligand. *Chem. Commun.* 49, 4785–4787.

Sharma, K.L., Agarwal, A., Misra, S., Kumar, A., Kumar, V., and Mittal, B. (2014). Association of genetic

variants of xenobiotic and estrogen metabolism pathway (CYP1A1 and CYP1B1) with gallbladder cancer susceptibility. *Tumor Biol.* 35, 5431–5439.

Smutna, V., Dieci, M.V., Lefebvre, C., Scott, V., Andre, F., and Fromigue, O. (2014). Is PYGM dysregulation involved in breast cancer cell metabolism.

Subramanian, A., Tamayo, P., Mootha, V.K., Mukherjee, S., Ebert, B.L., Gillette, M.A., Paulovich, A., Pomeroy, S.L., Golub, T.R., Lander, E.S., et al. (2005). Gene set enrichment analysis: A knowledge-based approach for interpreting genome-wide expression profiles. *Proc. Natl. Acad. Sci.* 102, 15545–15550.

Wasielewski, M., Elstrodt, F., Klijn, J.G.M., Berns, E.M.J.J., and Schutte, M. (2006). Thirteen new p53 gene mutants identified among 41 human breast cancer cell lines. *Breast Cancer Res. Treat.* 99, 97–101.